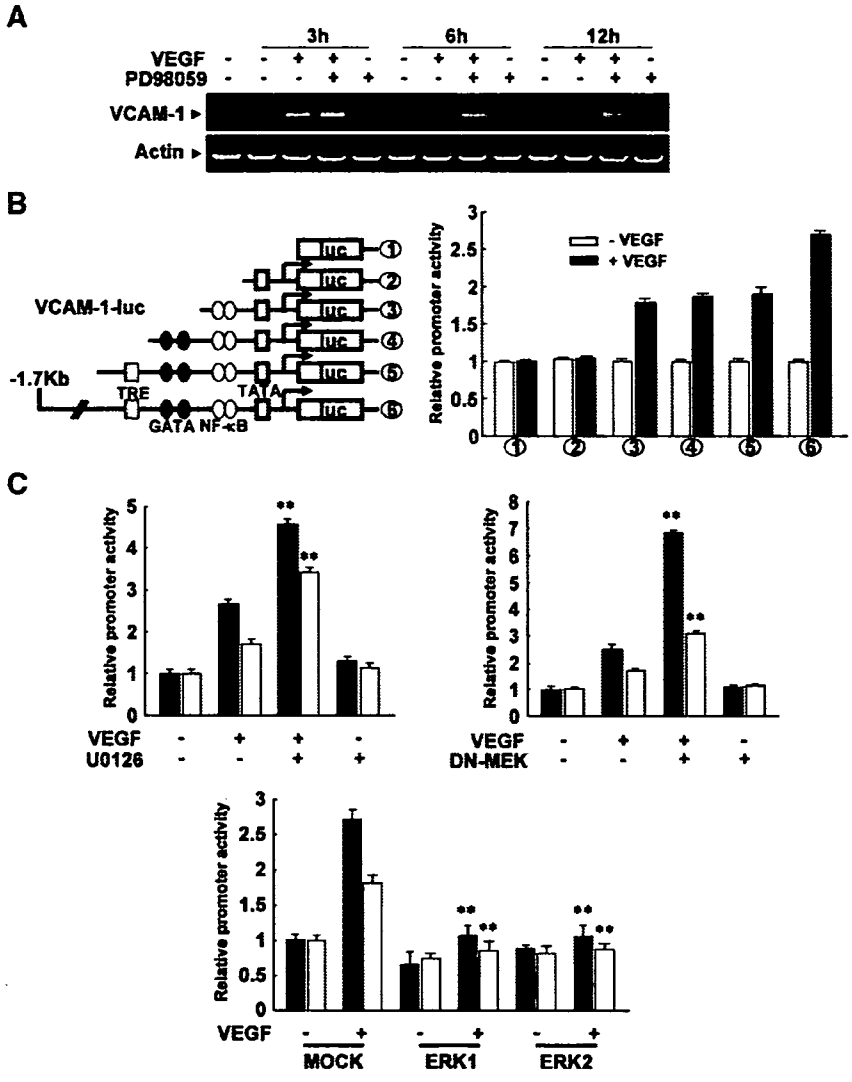

Fig. 2. ERK down-regulates VEGF-induced transcription of VCAM-1 by inhibiting NF-κB. (A) HUVECs were incubated for 30 min with or without 10 μM PD98059 and stimulated with 10 ng/ml VEGF for the indicated times. Total mRNAs were isolated and RT-PCR was performed with specific primers for human VCAM-1 as described in "Materials and methods". Actin served as an internal control. (B) HUVECs were cotransfected with a β-galactosidase plasmid and the various pVCAM-1-Luc deletion constructs as depicted. Twenty four hours later they were stimulated with 10 ng/ml VEGF for 24 h. (C) HUVECs were cotransfected with pVCAM-1-Luc (fragment 6: 1.8 kilobase pair, fragment 3: 329 bp), a β-galactosidase plasmid, and a dominant negative form of MEK1 (DN-MEK1), or wild form of ERKs (ERK1, 2). Twenty four hours after transfection, they were incubated with 10 ng/ml VEGF for 24 h. Luciferase activity was normalized to β-galactosidase activity. Data are means ± S.D. of luciferase light units relative to control untreated cells (set at 100%) in quadruplicate experiments. **, $P<0.01$ versus VEGF alone or MOCK + VEGF.

paraformaldehyde and permeabilized with 0.2% Triton X-100. After washing in phosphate-buffered saline, the slides were blocked with 3% bovine serum albumin for 1 h and the cells incubated with goat polyclonal anti-p65 antibody (Santa Cruz Biotechnology, Santa Cruz, CA) (1 : 100). After 2 h at 4 °C the cells were washed and incubated with anti-goat IgG-rhodamine (Santa Cruz) (1 : 100) for 1 h. The cells were then mounted with mounting medium and observed with a fluorescence microscope (Olympus).

2.11. Adhesion assays

HUVECs were plated on 2% gelatin-coated 96-well plates at a density of 1×10^4 cells/well and stimulated with VEGF for 8 h. Human U937 cells were then added (5×10^4 cells/ml, 200 μl/well) to the confluent HUVEC monolayers and incubated for 30 min. Thereafter the cells in the wells were washed out 3 times with PBS, fixed and stained with Diff-Quick (Baxter Healthcare Corp., McGraw Park, IL). The adherent cells in 5 randomly selected optical fields of each well were counted. Each experimental point was performed in duplicate and represents several independent conditions.

2.12. Western blotting

Cell lysates or immunoprecipitates were fractionated by SDS-PAGE and transferred to polyvinyldifluoride membranes. The blocked membranes were incubated with the appropriate

antibody, and the immunoreactive bands were visualized with a chemiluminescent reagent as recommended by Amersham Biosciences, Inc.

2.13. Statistical analysis

Data are presented as means±S.E., and statistical comparisons between groups were performed by 1-way ANOVA followed by Student's *t* test.

3. Results

3.1. Inhibition of ERK resulted in increased expression of VCAM-1 in response to VEGF

Vascular endothelial growth factor (VEGF), a well characterized angiogenic factor, also acts as a proinflammatory cytokine that produces enhanced leukocyte rolling and adhesion and increases endothelial permeability [29,30]. In endothelial cells, it strongly activates ERK and also induces expression of CAMs [31,32] in a NF-κB-dependent mechanism [31]. However, the level of CAM induction in response to VEGF is significantly lower, when compared in parallel, than those by TNF-α and IL-β, which show very little or negligible effect on ERK activation in endothelial cells (data not shown). Thus, it is supposed that the ERK pathway may interfere expression of inflammatory CAMs in response to proinflammatory factors in endothelium. To test this possibility, we first evaluated the role of ERK in VEGF-induced expression of inflammatory response gene such as VCAM-1 by employing MEK inhibitors, PD98059 and U0126, in endothelial cells. Treatment of HUVECs with VEGF enhanced VCAM-1 expression, with a maximum at 8 h (Fig. 1A). In the presence of 5 μM U0126, the effect of VEGF was markedly increased and prolonged up to 24 h (Fig. 1A). To confirm this inhibitory effect, we treated HUVECs with VEGF

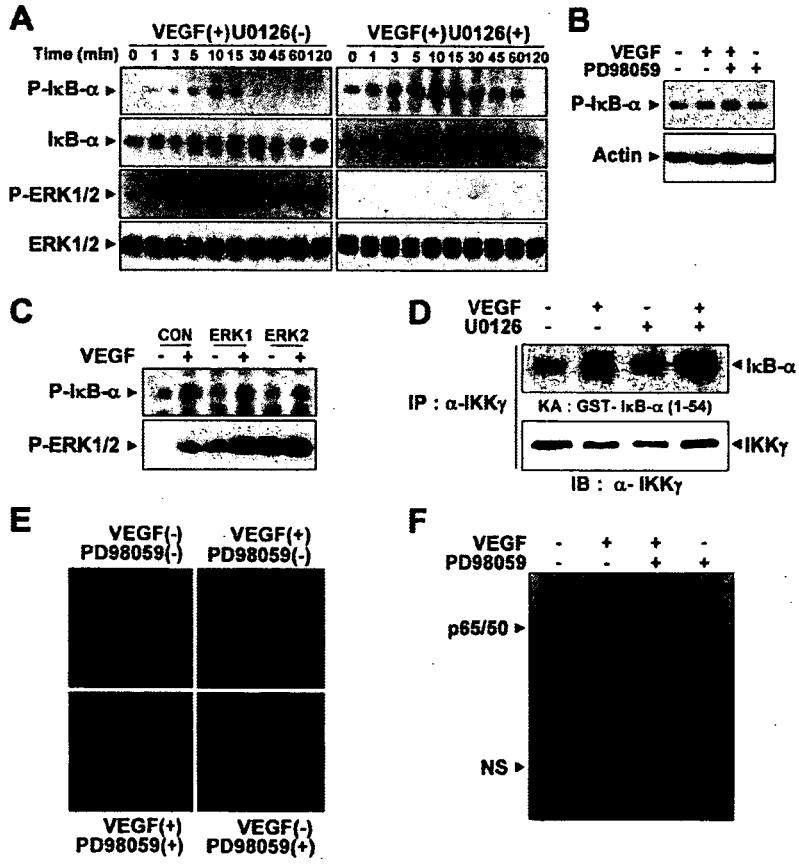

Fig. 3. Inhibition of ERK increases VEGF-induced IKK activity and nuclear translocation of NF-κB. (A) HUVECs were preincubated for 30 min with or without 5 μM U0126 and then stimulated with 10 ng/ml VEGF for the indicated times. Western blots were probed with anti-phospho-IκBα, anti-IκBα, anti-phospho-ERK, and anti-ERK antibodies. (B) HUVECs were preincubated for 30 min with or without 10 μM PD98059 and then stimulated with 10 ng/ml VEGF for 10 min. Western blots were probed with anti-phospho-IκBα and reprobed with an anti-actin antibody to verify equal loading of protein in each. (C) HUVECs were transfected with ERKs wild form (ERK1, 2) and then stimulated with VEGF for 10 min. Western blots were probed with anti-phospho-IκBα, and anti-phospho-ERK antibodies. (D) IKK activity was assessed by immune complex kinase assay as described in "Materials and methods". Recovery of IKK was assessed by immunoblotting for IKK-γ. (E) Immunocytochemical analysis of p65 localization. HUVECs were preincubated for 30 min with or without 10 μM PD98059 and then stimulated with 10 ng/ml VEGF for 30 min and subjected to immunocytochemistry as described in "Materials and methods". (F) HUVECs were preincubated for 30 min with or without 10 μM PD98059 and then stimulated with VEGF (20 ng/ml) for 30 min. Nuclear extracts were isolated and gel shift assay performed with a ^{32}P-radiolabeled NF-κB oligonucleotide of human VCAM-1.

for 10 min in the presence or absence of 5 μM U0126 and measured ERK activity by Western blotting with antibody against the phosphorylated form of ERK1/2 (p44 ERK1 and p42 ERK2). As shown in Fig. 1B, U0126 completely inhibited VEGF-induced ERK activation, whereas VEGF-induced VCAM-1 expression was increased (Fig. 1B). Pretreatment with the other MEK inhibitor, PD98059, also augmented VEGF-induced VCAM-1 expression, while reducing ERK activation (Fig. 1B). U0126 or PD98059 alone had no effect on VCAM-1 expression (Fig. 1B). In addition, the U0126-induced increase in VEGF-induced VCAM-1 expression was dose-dependent, and inversely related to ERK activity (Fig. 1C). FACScan analysis confirmed that U0126 augmented VEGF-induced expression of VCAM-1 on the cell surface of HUVECs (Fig. 1D).

To further confirm that the enhancement of VEGF-induced VCAM-1 expression by the inhibitors was due specifically to inhibition of ERK signaling, we determined the effects of a dominant negative MEK1 (DN-MEK1) mutant and two types of wild type ERK (ERK1 and ERK2). In agreement with the results with chemical inhibitors, Western blot analysis showed that overexpression of DN-MEK1 reduced VEGF-induced ERK phosphorylation, and increased the induction of VCAM-1 by VEGF (Fig. 1E). Moreover, there was a small increase in basal VCAM-1 expression in the cells expressing DN-MEK-1 (Fig. 1E). In contrast, HUVECs overexpressed with either wild type ERK1 or ERK2 increased ERK phosphorylation, and decreased VCAM-1 expression in response to VEGF (Fig. 1F). These results confirm that the ERK pathway inhibits VEGF signaling leading to VCAM-1 expression in endothelial cells.

3.2. ERK down-regulates VEGF-induced transcription of VCAM-1 by inhibiting NF-κB

To determine whether ERK inhibits VEGF-activated transcription of VCAM-1 in endothelial cells, we performed semi-quantitative RT-PCR and assayed transcription from the VCAM-1 luciferase plasmids described in Materials and methods. Treatment of HUVECs with VEGF in the absence of ERK inhibitor induced the appearance of VCAM-1 mRNA within 3 h, and the mRNA declined thereafter (Fig. 2A). In the presence of 10 μM PD98059, the level of VCAM-1 mRNA induced by VEGF was increased and sustained up to 12 h (Fig. 2A). These changes could result either from new synthesis or from increased mRNA stability. Pretreatment with actinomycin D, an inhibitor of transcription, almost completely prevented the increase of VCAM-1 mRNA in response to PD98059 (data not shown), suggesting that ERK inhibits VEGF-activated transcription. The human VCAM-1 promoter (1.7 kb) includes binding sites for NF-κB, TRE, and GATA [26]. Although previous report have implicated NF-κB in VEGF-induced VCAM-1 expression in endothelial cells [26,33], its precise role in activation of the VCAM-1 promoter has not been determined. To identify the cis elements involved, we serially deleted the 1.7 kb VCAM-1 promoter and introduced the resulting plasmids into HUVECs. As shown in Fig. 2B, deletion of the 5′ 1.2 kb region substantially reduced the response to VEGF, but further deletion of the TRE and GATA sites had no appreciable effect. Deletion of the proximal NF-κB binding sites located about 65 and 75 bp upstream of the transcription start site resulted in complete lose of responsiveness to VEGF. These results demonstrate that the NF-κB motifs on the VCAM-1 promoter are important for VEGF-mediated activation of the VCAM-1 promoter, together with an unidentified element in the 5′ 1.2 kb upstream region.

To further confirm the role of ERK in VEGF-induced VCAM-1 transcription, HUVECs were transiently transfected with a VCAM-1 luciferase plasmid harboring the VCAM-1 promoter region. As shown in Fig. 2C, VEGF induced VCAM-1-dependent transcriptional activity, and this was increased by pretreatment with 5 μM U0126, or by introducing DN-MEK-1, but abrogated by ERK or ERK2. These results confirm that ERK controls VEGF-mediated expression of VCAM-1 at the transcriptional level. Since the NF-κB motifs play a significant role in VEGF-induced transcription of VCAM-1, it seemed possible that ERK suppressed activation of NF-κB by VEGF. Indeed, VEGF-induced transcription from a luciferase plasmid containing the proximal NF-κB binding sites of the VCAM-1 promoter was markedly increased by U0126 and DN-MEK1, and almost completely blocked by ERK1 or ERK2 (Fig. 2C). These results suggest that ERK inhibits VEGF-induced transcription of VCAM-1 mRNAs at least in part by suppressing transcription from the NF-κB elements in the VCAM-1 promoter.

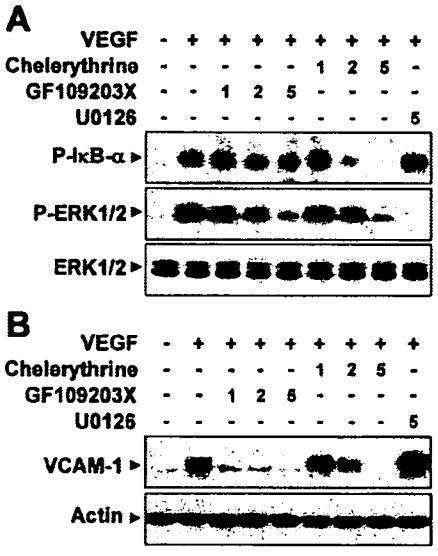

Fig. 4. PKC mediates both IκBα phosphorylation and ERK activation by VEGF. HUVECs were preincubated for 30 min with or without GF109203X, chelerythrine chloride (1, 2, or 5 μM) or 5 μM U0126 and then stimulated with 10 ng/ml VEGF for 10 min (A) or 8 h. (B). Western blots were probed with anti-phospho-IκBα, anti-IκBα, anti-phospho-ERK, and anti-ERK antibodies (A), and anti-VCAM-1 and anti-actin antibodies (B). Actin was used to verify equal loading of protein.

3.3. Inhibition of ERK increases VEGF-induced IKK activity and nuclear translocation of NF-κB

The activated form of NF-κB is a heterodimer that usually consists of two proteins, a p65 (also called relA) subunit and a p50 subunit [7]. In the inactive state, NF-κB is found in the cytoplasm bound to IκBα, which prevents it from entering the nuclei [7,34]. Activation of NF-κB is preceded by the phosphorylation, ubiquitination, and proteolytic degradation of IκBα [34]. Therefore, we examined the effect of ERK inhibitors on VEGF-induced IκBα phosphorylation and degradation by Western blotting with antibodies against phospho-IκBα (Ser-32) and IκBα. As shown in Fig. 3A, VEGF treatment led to phosphorylation of IκBα and maximal activation was observed after 10 min. Pretreatment with U0126 substantially enhanced VEGF-induced IκBα phosphorylation. Moreover, while degradation of IκBα was barely detectable after stimulation with VEGF on its own,

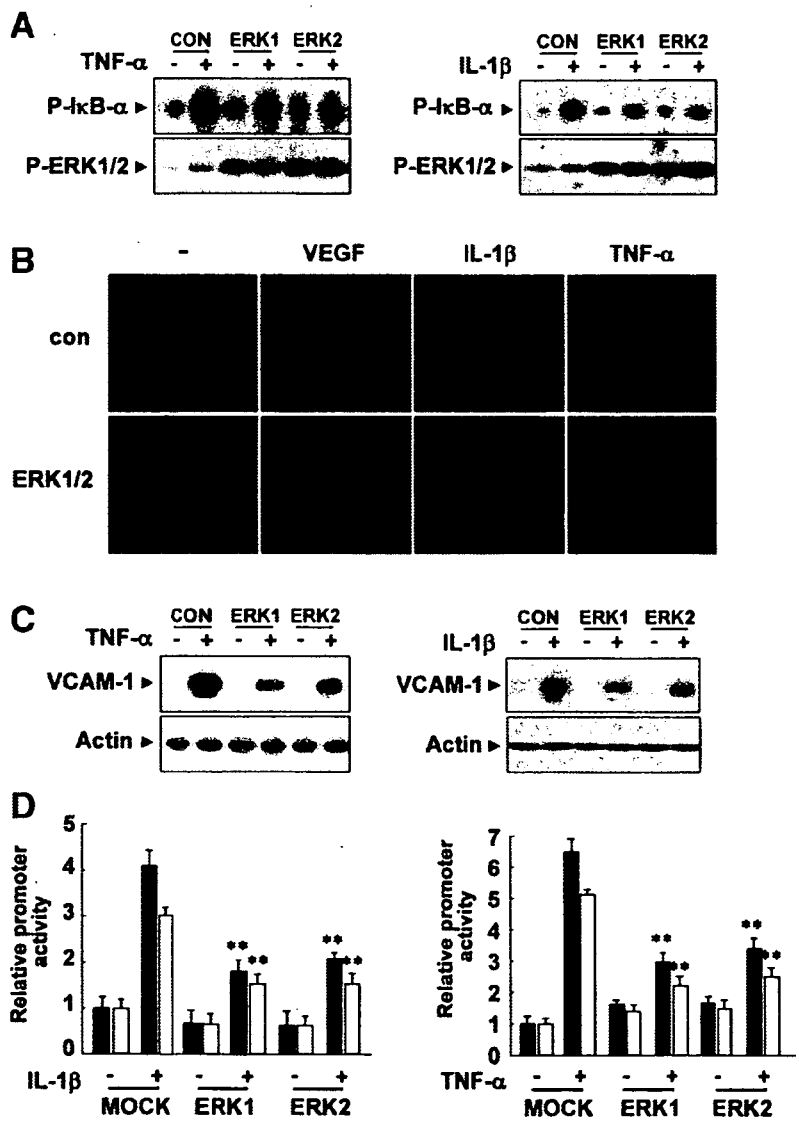

Fig. 5. Overexpression of ERK suppresses NF-κB activation and VCAM-1 expression in response to IL-1β and TNF-α. (A) HUVECs were transfected with ERK wild form (ERK1, 2) and then stimulated with 10 ng/ml TNF-α or 50 units/ml IL-1β for 10 min. Western blots were probed with anti-phospho-IκBα and anti-phospho-ERK antibodies. (B) Immunocytochemical analysis of p65 localization. HUVECs were transfected with ERKs wild form (ERK1, 2) and then stimulated with 10 ng/ml VEGF, 10 ng/ml TNF-α or 50 units/ml IL-1β for 30 min and subjected to immunocytochemistry as described in "Materials and methods". (C) HUVECs were transfected with ERKs wild form (ERK1, 2) and then stimulated with 10 ng/ml TNF-α or 50 units/ml IL-1β for 8 h. Western blots were probed with anti-VCAM-1 and reprobed with an anti-actin antibody to verify equal loading of protein in each. (D) HUVECs were cotransfected with pVCAM-1-Luc (fragment 6: 1.8 kilobase pair, fragment 3: 329 bp), a β-galactosidase plasmid, and a ERKs wild form (ERK1, 2). Twenty four hours after transfection, they were incubated with 10 ng/ml TNF-α or 50 units/ml IL-1β for 24 h. Luciferase activity was normalized to β-galactosidase activity. Data are means±S.D. of luciferase light units relative to control untreated cells (set at 100%) in quadruplicate experiments. **, $P<0.01$ versus MOCK+IL-1β or MOCK+TNF-α.

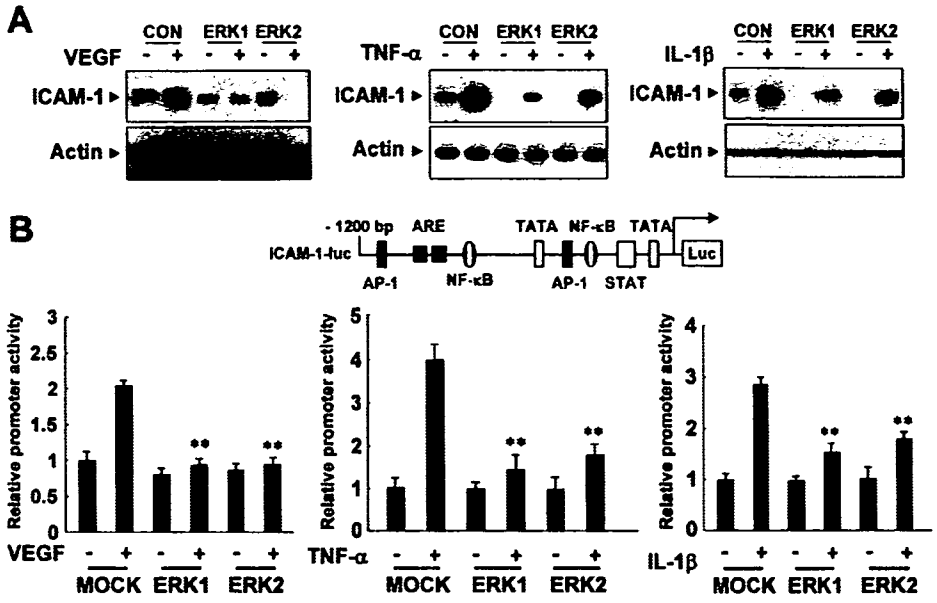

Fig. 6. ERK reduces endothelial ICAM-1 expression in response to VEGF, IL-1β, and TNF-α. (A) HUVECs were transfected with ERKs wild form (ERK1, 2) and then stimulated with 10 ng/ml VEGF, 10 ng/ml TNF-α or 50 units/ml IL-1β for 8 h. Western blots were probed with anti-ICAM-1 and reprobed with an anti-actin antibody to verify equal loading of protein in each. (B) HUVECs were cotransfected with pICAM-1-Luc (1.2 kilobase pair), a β-galactosidase plasmid, and a ERKs wild form (ERK1, 2). Twenty four hours after transfection, they were incubated with 10 ng/ml VEGF, 10 ng/ml TNF-α or 50 units/ml IL-1β for 24 h. Luciferase activity was normalized to β-galactosidase activity. Data are means±S.D. of luciferase light units relative to control untreated cells (set at 100%) in quadruplicate experiments. **, $P<0.01$ versus MOCK+VEGF, MOCK+IL-1β or MOCK+TNFα.

when U0126 was added, the level of IκBα markedly decreased following 30 min of VEGF treatment (Fig. 3A). We also observed that PD98059 increased the effect of VEGF on phosphorylation and subsequent degradation of IκBα in a manner similar to U0126 (Fig. 3B). In contrast, VEGF-induced IκBα phosphorylation was almost completely abrogated by overexpression of ERK1 or ERK2 (Fig. 3C). To further confirm the effect of U0126 on VEGF-induced IκBα phosphorylation, the IκB kinase (IKK) enzymatic assay was performed. IKK is a complex composed of three subunits: IKKα (IKK1), IKKβ (IKK2), and IKKγ (NEMO, IKKAP) [11]. IKK activity was determined in anti-IKKγ immunoprecipitates as described [28]. Cell stimulation with VEGF activated the ability of IKK to phosphorylate GST-IκBα (Fig. 3D). This VEGF-induced IKK activation was significantly increased by pretreatment of U0126 (Fig. 3D).

The dissociation of NF-κB from IκBα results in translocation of NF-κB to the nucleus, where it binds to specific sequences in the promoter regions of target genes. We next determined the effect of ERK inhibitors on VEGF-induced nuclear translocation and NF-κB DNA binding activity. VEGF caused nuclear translocation of the p65 subunit of NF-κB and this was significantly increased by pretreatment with PD98059 (Fig. 3E). Furthermore binding to target NF-κB oligonucleotides was also markedly augmented by pretreatment with PD98059 (Fig. 3F). PD98059 on its own had no effect on nuclear translocation and NF-κB DNA binding activity (Fig. 3E and F). Collectively, these results suggest that ERK suppresses VEGF-induced NF-κB activation by blocking the VEGF signaling pathway leading to IκBα phosphorylation.

3.4. PKC mediates both IκBα phosphorylation and ERK activation by VEGF

Our data indicate that VEGF induces both IκBα phosphorylation and ERK activation in endothelial cells. It was of interest to identify the upstream signaling molecules that lead to IKK and ERK activation. A previous study suggested the involvement of PKC in NF-κB activation leading to endothelial CAM expression [31,35,36]. We therefore examined the role of PKC in IκBα phosphorylation by employing two PKC inhibitors, GF109203X and chelerythrine chloride, and, in parallel, compared the effect of these inhibitors on VEGF-induced ERK activation. As shown in Fig. 4A, both IκBα phosphorylation and ERK activation in response to VEGF were inhibited by GF109203X and chelerythrine chloride, indicating that PKC lies upstream of both IKK and ERK. Under the same condition, U0126 completely inhibited ERK activation in response to VEGF, and increased the VEGF effect on IκBα phosphorylation (Fig. 4A). Similarly, VEGF-induced VCAM-1 expression was blocked by GF109203X and chelerythrine chloride, but increased by U0126 (Fig. 4B). These results suggest that in the VEGF signaling pathway PKC provides a positive signal activating IKK and ERK, a negative signal.

3.5. Overexpression of ERK suppresses NF-κB activation and VCAM-1 expression in response to IL-1β and TNF-α

The role of ERK pathway in other cytokine-induced NF-κB activation was explored. Unlikely to VEGF, IL-1β and TNF-α

did not significantly induce ERK activation in HUVECs in contrast to their strong stimulatory activity on NF-κB. Consistently, inhibition of ERK by pretreatment of HUVECs with 5 μM U0126 did not further increase IκBα phosphorylation in response to either IL-1β or TNF-α (data not shown). However, overexpression of either wild type ERK1 or ERK2 markedly reduced both IL-1β-and TNF-α-induced IκBα phosphorylation (Fig. 5A). In addition, nuclear translocation of p65 subunit of NF-κB induced by either IL-1β or TNF-α was blocked by overexpression of ERKs (Fig. 5B). In agreement, both IL-1β and TNF-α increased endothelial VCAM-1 expression in a NF-κB dependent manner as shown in a promoter assay and these responses were significantly abrogated by overexpression of either ERK1 or ERK2 (Fig. 5C and D). These results raised the possibility that ERK negatively regulates NF-κB-dependent gene expression in endothelial cells through inhibiting the IκBα phosphorylation pathway stimulated by various agonists.

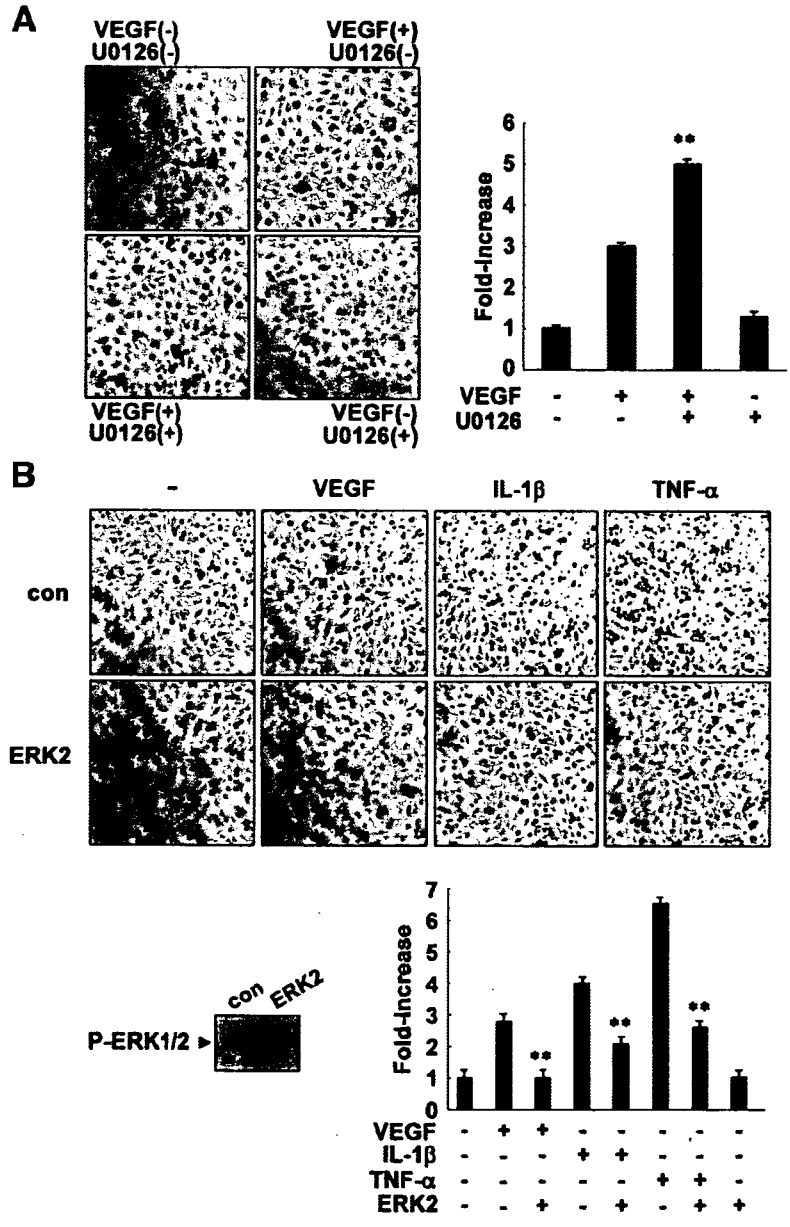

Fig. 7. ERK inhibitors increase VEGF-Induced leukocyte adhesion to endothelial cells. (A) HUVECs were preincubated for 30 min with or without 5 μM U0126 and then stimulated with 10 ng/ml VEGF for 8 h. (B) ERK2 lentiviral vectors were added to cell cultures at varying multiplicities of infection (MOIs ≈1–50). At 18 h, cells were washed and medium was replaced. HUVECs were stimulated with 10 ng/ml VEGF, 10 ng/ml TNF-α or 50 units/ml IL-1β for 8 h. Thereafter adhesion to U937 human monocytes was measured as described in "Materials and methods." Data are means±S.D. of adhesion relative to control untreated cells (set at 100%) in quadruplicate experiments. **, $P<0.01$ versus VEGF, IL-1β or TNF-α.

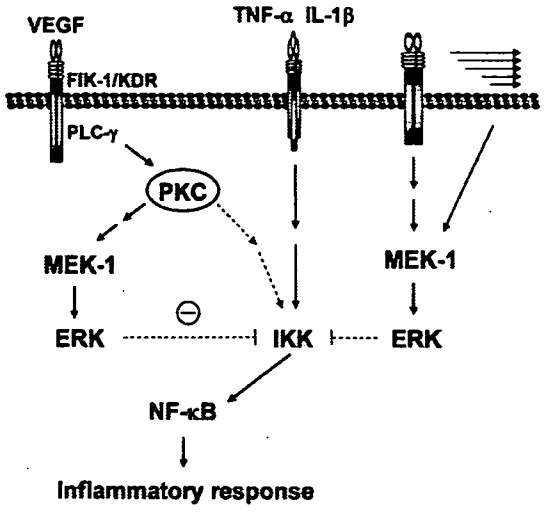

Fig. 8. Potential mechanism supporting anti-inflammatory role of ERK in the vascular wall.

3.6. ERK reduces endothelial ICAM-1 expression in response to VEGF, IL-1β, and TNF-α

We further confirmed the role of ERK pathway on expression of other inflammatory genes in endothelial cells. ICAM-1 is one of representative endothelial cell adhesion molecules expressed in a NF-κB dependent mechanism. As expected, the protein level of ICAM-1 on HUVECs was increased by either treatment of VEGF, IL-1β or TNF-α (Fig. 6A). All these increases were almost completely or markedly inhibited by overexpression of either ERK1 or ERK2 (Fig. 6A). Consistently, ICAM-1-dependent transcriptional activities induced by these cytokines were inhibited by overexpression of ERK1 or ERK2 (Fig. 6B).

3.7. ERK inhibitors increase VEGF-Induced leukocyte adhesion to endothelial cells

Expression of CAMs, such as ICAM-1 and VCAM-1, on the surface of endothelial cells is required for endothelial–leukocyte interaction. Since inhibition of the ERK pathway increases the effect of VEGF on endothelial CAM expression, we tested whether the ERK inhibitor stimulates leukocyte adhesion to endothelial cells. HUVECs were exposed to 10 ng/ml VEGF for 8 h and then co-cultured with human monocytic U937 cells for an additional 1 h. As shown in Fig. 7, the adhesion of U937 cells to HUVECs was increased by VEGF, and this effect was accentuated by pretreatment with 5 μM U0126 (Fig. 7A). U0126 alone, on the other hand, had no effect (Fig. 7A). In contrast, overexpression of ERK2 markedly reduced VEGF-induced adhesion of U937 cells to HUVECs (Fig. 7B). Moreover, both IL-1β-and TNF-α-induced monocyte–endothelial cell interaction was also significantly reduced by overexpression of ERK2 (Fig. 7B).

4. Discussion

Unveiling of endothelial NF-κB activation is pivotal for understanding the inflammatory reaction and the pathogenesis of inflammatory vascular diseases. A large number of studies have revealed the presence of a number of cellular stimuli, including inflammatory cytokines and oscillating shear stress, that lead to the endothelial NF-κB activation [10,37]. Conversely, factors such as angiopoietin-1, bFGF, hepatocyte growth factor (HGF), and normal lamina shear stress were shown to suppress NF-κB activation [38,39]. However, despite of a number of reports, precise understanding of their action mechanisms in the vasculature remains still unclear. Importantly, the present study demonstrates the novel role of ERK in controlling endothelial NF-κB activation and inflammatory gene expression.

Our data showed that inhibition of ERK increased VCAM-1 expression in response to VEGF stimulation, but that ERK inhibitors alone had no significant effect. This indicates that inhibition of ERK itself is incapable of stimulating VCAM-1 expression in endothelial cells, and suggests that VEGF sets in train both positive and negative signals related to VCAM-1 expression and that ERK may serve as an internal suppressor of the positive signal. Using two PKC inhibitors, it is clearly demonstrated that VEGF stimulates both ERK and IKK through PKC that lies downstream of KDR/Flk-1. Since ERK inhibits IKK activation by VEGF (Fig. 4), PKC seems to transmit both positive and negative signals involved in IKK activation. Therefore, the relatively weak activation of IKK and expression of inflammatory genes by VEGF is likely to be due to the concomitant activation of ERK. Similar phenomenon was observed in TNF-related activation-induced cytokine (TRANCE)-induced NF-κB activation and VCAM-1 expression. TRANCE stimulated ERK, IκBα phosphorylation, and transcriptional activity of NF-κB in HUVECs [40,41]. Pretreatment of the ERK inhibitors significantly enhanced TRANCE-induced NF-κB activation and VCAM-1 expression (data not shown), suggesting the suppressive role of concomitantly activated ERK in the cytokine-induced NF-κB pathway in endothelial cells.

Unlikely to VEGF, IL-1β and TNF-α had little effect on ERK activation in HUVECs, but they much strongly induced IKK activation and VCAM-1 expression compared to VEGF. The effects of IL-1β and TNF-α on IKK activation and VCAM-1 expression was very slightly increased by the ERK inhibitor (data not shown) but markedly suppressed by overexpression of ERK1 or ERK2. We also tested the effect of bFGF and EGF on VCAM-1 expression in HUVECs. These two growth factors markedly stimulated ERK activation in HUVECs, but did not induce VCAM-1 expression. In addition, ERK inhibitors had no significant effect on VCAM-1 expression (data not shown), presumably because these growth factors do not activate the NF-κB signaling pathway. We have recently reported that HGF counteracts VEGF-induced endothelial CAM expression through inhibiting IKK-mediated NF-κB activation [42]. HGF itself was unable to induce NF-κB activation but strongly stimulated ERK activation in endothelial cells (data not shown).

In deed, it is observed that pretreatment of the ERK inhibitor prior to HGF administration results in reversing the inhibitory effect of HGF on VEGF-induced IκBα phosphorylation and VCAM-1 expression (data not shown). Although the precise mechanism engaged in agonists-dependent activation or inhibition of NF-κB pathway remains elusive, it is at least in part suggested that the cellular level of ERK activity may be one of crucial components to control IKK-mediated NF-κB activation in endothelial cells. Western blotting with antibodies against phospho-IκBα (Ser-32) and IκBα revealed that the ERK inhibitors increase IκBα phosphorylation at Ser-32 and degradation in response to VEGF (Fig. 4). Conversely, forced elevation of ERK activity in HUVECs resulted in the inhibition of phosphorylation of IκBα on Ser-32 by VEGF, IL-1β, and TNF-α. IKK exists as a high molecular complex containing two kinase subunits, IKKα (IKK1) and IKKβ (IKK2), and a regulatory subunit, NEMO [13]. The phosphorylation of IκBα on Ser-32 and Ser-36 is mediated mainly by the kinase activity of IKKβ and led to its proteolytic degradation and subsequent nuclear translocation of NF-κB [13]. Therefore, ERK is most likely to inhibit the canonical NF-κB pathway that involves IKK-mediated IκBα phosphorylation in endothelial cells.

In conclusion, our present data apparently demonstrate a novel function of ERK as a curb of endothelial NF-κB activation with possible mechanism (Fig. 8). Indeed, elevation of ERK activity in endothelial cells significantly suppressed expression of NF-κB-dependent genes such as ICAM-1 and VCAM-1 in response to cytokine stimulation. These effects were functionally correlated with decreased endothelial cell–monocyte interaction. Although the further study is required to prove the anti-inflammatory nature of ERK in more complex in vivo environment, our findings suggest that ERK activity constitutively or transiently induced by normal laminar flow or various endothelial stimuli may serve as a negative regulator of vascular inflammation by suppressing endothelial NF-κB activation. Therefore, measuring the existence of ERK activity in vascular endothelial cells may be useful for predicting the feasibility and potency of inflammatory reactions in the vascular wall.

Acknowledgments

This work was supported by a Next Generation Growth Engine Program Grant and Vascular System Research Center Grant from the Korean Ministry of Science and Technology.

References

[1] H. Ulbrich, E.E. Eriksson, L. Lindbom, Trends Pharmacol. Sci. 24 (2003) 640.
[2] D. Vestweber, Curr. Opin. Cell Biol. 14 (2002) 587.
[3] W.A. Muller, Lab Invest. 82 (2002) 521.
[4] P. Xia, J.R. Gamble, K.A. Rye, L. Wang, C.S. Hii, P. Cockerill, Y. Khew-Goodall, A.G. Bert, P.J. Barter, M.A. Vadas, Proc. Natl. Acad. Sci. U. S. A. 95 (1998) 14196.
[5] K.T. Piercy, R.L. Donnell, S.S. Kirkpatrick, C.H. Timaran, S.L. Stevens, M.B. Freeman, M.H. Goldman, J. Surg. Res. 105 (2002) 215.
[6] S. Zeuke, A.J. Ulmer, S. Kusumoto, H.A. Katus, H. Heine, Cardiovasc. Res. 56 (2002) 126.
[7] J. Peter, D.M. Barnes, Sc. D, Michael Karin, N. Engl. J. Med. 336 (1997) 1066.
[8] P.A. Baeuerle, T. Henkel, Annu. Rev. Immunol. 12 (1994) 141.
[9] C. Maaser, S. Schoeppner, T. Kucharzik, M. Kraft, E. Schoenherr, W. Domschke, N. Luegering, Clin. Exp. Immunol. 124 (2001) 208.
[10] J.T. Wu, J.G. Kral, J. Surg. Res. 123 (2005) 158.
[11] Y. Yamamoto, R.B. Gaynor, Trends Biochem. Sci. 29 (2004) 72.
[12] P. Viatour, M.P. Merville, V. Bours, A. Chariot, Trends Biochem Sci. 30 (2005) 43.
[13] M.S. Ayden, S. Hosh, Genes Dev. 18 (2004) 2195.
[14] E. Majewska, E. Paleolog, Z. Baj, U. Kralisz, M. Feldmann, H. Tchorzewski, Scand. J. Immunol. 45 (1997) 385.
[15] H. Zhang, A.C. Issekutz, Am. J. Pathol. 160 (2002) 2219.
[16] M. Kaneki, S. Kharbanda, P. Pandey, K. Yoshida, M. Takekawa, J.R. Liou, R. Stone, D. Kufe, Mol. Cell. Biol. 19 (1999) 461.
[17] R. Datta, K. Yoshinaga, M. Kaneki, P. Pandey, D. Kufe, J. Biol. Chem. 275 (2000) 41000.
[18] J.H. Je, J.Y. Lee, K.J. Jung, B. Sung, E.K. Go, B.P. Yu, H.Y. Chung, FEBS Lett. 566 (2004) 183.
[19] C. Schmidt, B. Peng, Z. Li, G.M. Sclabas, S. Fujioka, J. Niu, M. Schmidt-Supprian, D.B. Evans, J.L. Abbruzzese, P.J. Chiao, Mol. Cell. 12 (2003) 1287.
[20] J.R. Burke, J. Strnad, Biochem. Biophys. Res. Commun. 293 (2002) 1508.
[21] P.E. Hughes, M.W. Renshaw, M. Pfaff, J. Forsyth, V.M. Keivens, M.A. Schwartz, M.H. Ginsberg, Cell 88 (1997) 521.
[22] R. Gum, H. Wang, E. Lengyel, J. Juarez, D. Boyd, Oncogene 14 (1997) 481.
[23] D. Besser, M. Presta, Y. Nagamine, Cell Growth Differ. 6 (1995) 1009.
[24] E. Meylan, F. Martinon, M. Thome, M. Gschwendt, J. Tschopp, EMBO Rep. 3 (2002) 1201.
[25] E.A. Jaffe, R.L. Nachman, C.G. Becker, C.R. Minick, J. Clin. Invest. 52 (1973) 2745.
[26] T. Minami, W.C. Aird, J. Biol. Chem. 276 (2001) 47632.
[27] D. Cefai, E. Simeoni, K.M. Ludunge, R. Driscoll, L.K. von Segesser, L. Kappenberger, G. Vassalli, J. Mol. Cell. Cardiol. 38 (2005) 333.
[28] Y. Takada, A. Mukhopadhyay, G.C. Kundu, G.H. Mahabeleshwar, S. Singh, B.B. Aggarwal, J. Biol. Chem. 278 (2003) 24233.
[29] M.A. Proescholdt, S. Jacobson, N. Tresser, E.H. Oldfield, M.J. Merrill, J. Neuropathol. Exp. Neurol. 61 (2002) 914.
[30] S.D. Croll, J.H. Goodman, H.E. Scharfman, Adv. Exp. Med. Biol. 548 (2004) 57.
[31] I. Kim, S.O. Moon, S.H. Kim, H.J. Kim, Y.S. Koh, G.Y. Koh, J. Biol. Chem. 276 (2001) 7614.
[32] I. Kim, S.O. Moon, S.K. Park, S.W. Chae, G.Y. Koh, Circ. Res. 89 (2001) 477.
[33] H.J. Park, Y.W. Lee, B. Hennig, M. Toborek, Nutr. Cancer 41 (2001) 126.
[34] V. Dixit, T.W. Mak, Cell 111 (2002) 615.
[35] K. Page, J. Li, L. Zhou, S. Iasvovskaia, K.C. Corbit, J.W. Soh, I.B. Weinstein, A.R. Brasier, A. Lin, M.B. Hershenson, J. Immunol. 170 (2003) 5681.
[36] T. Minami, M.R. Abid, J. Zhang, G. King, T. Kodama, W.C. Aird, J. Biol. Chem. 278 (2003) 6976.
[37] G.P. Sorescu, M. Sykes, D. Weiss, M.O. Platt, A. Saha, J. Hwang, N. Boyd, Y.C. Boo, J.D. Vega, W.R. Taylor, H. Jo, J. Biol. Chem. 278 (2003) 31128.
[38] E. Eng, B.J. Ballermann, Microvasc. Res. 65 (2003) 137.
[39] B.H. Jeon, F. Khanday, S. Deshpande, A. Haile, M. Ozaki, K. Irani, Circ. Res. 92 (2003) 586.
[40] Y.M. Kim, Y.M. Kim, Y.M. Lee, H.S. Kim, J.D. Kim, Y. Choi, K.W. Kim, S.Y. Lee, Y.G. Kwon, J. Biol. Chem. 277 (2002) 6799.
[41] J.K. Min, Y.M. Kim, S.W. Kim, M.C. Kwon, Y.Y. Kong, I.K. Hwang, M. H. Won, J. Rho, Y.G. Kwon, J. Immunol. 175 (2005) 531.
[42] J.K. Min, Y.M. Lee, J.H. Kim, Y.M. Kim, S.W. Kim, S.Y. Lee, Y.S. Gho, G.T. Oh, Y.G. Kwon, Circ. Res. 96 (2005) 300.

LETTERS

p53-induced inhibition of Hif-1 causes cardiac dysfunction during pressure overload

Masanori Sano[1]*, Tohru Minamino[1]*, Haruhiro Toko[1], Hideyuki Miyauchi[1], Masayuki Orimo[1], Yingjie Qin[1], Hiroshi Akazawa[1], Kaoru Tateno[1], Yosuke Kayama[1], Mutsuo Harada[1], Ippei Shimizu[1], Takayuki Asahara[2], Hirofumi Hamada[3], Shuhei Tomita[4], Jeffrey D. Molkentin[5], Yunzeng Zou[6] & Issei Komuro[1]

Cardiac hypertrophy occurs as an adaptive response to increased workload to maintain cardiac function[1]. However, prolonged cardiac hypertrophy causes heart failure[2], and its mechanisms are largely unknown. Here we show that cardiac angiogenesis is crucially involved in the adaptive mechanism of cardiac hypertrophy and that p53 accumulation is essential for the transition from cardiac hypertrophy to heart failure. Pressure overload initially promoted vascular growth in the heart by hypoxia-inducible factor-1 (Hif-1)-dependent induction of angiogenic factors, and inhibition of angiogenesis prevented the development of cardiac hypertrophy and induced systolic dysfunction. Sustained pressure overload induced an accumulation of p53 that inhibited Hif-1 activity and thereby impaired cardiac angiogenesis and systolic function. Conversely, promoting cardiac angiogenesis by introducing angiogenic factors or by inhibiting p53 accumulation developed hypertrophy further and restored cardiac dysfunction under chronic pressure overload. These results indicate that the anti-angiogenic property of p53 may have a crucial function in the transition from cardiac hypertrophy to heart failure.

During the development of cardiac hypertrophy, it has been postulated that a mismatch between the number of capillaries and the size of cardiomyocytes develops, leading to myocardial hypoxia[3,4]. There are various reports indicating a potential relationship between cardiac angiogenesis, cardiac hypertrophy and cardiac function[5–7]. We thus proposed that cardiac angiogenesis might contribute to the development of cardiac hypertrophy and that its impairment might induce heart failure.

We first established a hypertrophy model that shows cardiac dysfunction at chronic stage by performing a severe transverse aorta constriction (TAC). In this model, cardiac hypertrophy gradually developed, reached a peak on day 14 after TAC and decreased afterwards (Fig. 1a–d). Fractional shortening was preserved until day 14 and significantly decreased on day 28 with left ventricular dilation and increased cardiac fibrosis (Fig. 1d, e, and Supplementary Fig. 1a, b). These results suggest that pressure overload initially induced 'adaptive' hypertrophy (days 1–14) with preserved cardiac function; however, this adaptive mechanism could not protect the hypertrophied heart against sustained pressure overload, resulting in systolic dysfunction (days 14–28). The number of microvessels per cardiomyocyte increased until day 14 and decreased thereafter (Fig. 1b, c). The number of bromodeoxyuridine (BrdU)-positive endothelial cells, but not that of BrdU-positive cardiomyocytes, was significantly increased (Supplementary Fig. 1c). Consistent with these results was our observation that the expression of angiogenic factors such as vascular endothelial growth factor (VEGF) and angiopoietin-1 (Ang-1) was upregulated in the early phase and decreased in the late phase (Fig. 1f, g).

To explain the role of angiogenesis in the development of cardiac hypertrophy, we examined the effects of TNP-470, an inhibitor of angiogenesis[8], on cardiac hypertrophy. TNP-470 suppressed the increase in the number of microvessels in the heart of mice that had undergone TAC (Fig. 2a). TAC-induced hypertrophy was almost completely inhibited by the treatment with TNP-470 (Fig. 2a, b). Administration of TNP-470 to mice significantly impaired cardiac function at 2 weeks after TAC (Fig. 2b). Similar inhibitory effects of TNP-470 were observed in other models of cardiac hypertrophy such as an angiotensin II infusion model (Supplementary Fig. 2a–d). These results suggest that cardiac angiogenesis is crucially involved in preserving cardiac function as well as in developing cardiac hypertrophy.

To examine whether promoting angiogenesis prevents the transition from cardiac hypertrophy towards heart failure, we introduced adenoviral vectors encoding VEGF and Ang-1 directly into the heart and produced pressure overload. Introduction of angiogenic factors enhanced an increase in the number of microvessels compared with that of LacZ after TAC (Fig. 2c). Cardiac hypertrophy was further developed and its function was preserved in the VEGF/Ang-1 group at 4 weeks after TAC (Fig. 2c, d). Conversely, the introduction of a soluble form of Flt-1, an inhibitor of angiogenesis[9], into the thigh muscle markedly reduced cardiac hypertrophy as well as the number of microvessels compared with that of LacZ, and suppression of this adaptive response caused a further decline in cardiac systolic function at 4 weeks after TAC (Fig. 2c, d). These results indicate that cardiac angiogenesis, which is induced in the early adaptive phase, may be sufficient to maintain cardiac function and that the angiogenesis becomes insufficient to keep the function of hypertrophied hearts in the maladaptive phase, presumably because of decreased expression of angiogenic factors.

Cardiomyocyte hypertrophy has been thought to increase diffusion distance, resulting in reduced oxygen supply in the myocardium. Neovascularization associated with cardiac hypertrophy may be attributable to angiogenic factors in cardiomyocytes being upregulated by hypoxia. We therefore examined the expression of Hif-1α, a key transcription factor for the hypoxic induction of angiogenic

[1]Department of Cardiovascular Science and Medicine, Chiba University Graduate School of Medicine, 1-8-1 Inohana, Chuo-ku, Chiba 260-8670, Japan. [2]Stem Cell Translational Research, Kobe Institute of Biomedical Research and Innovation/RIKEN Center for Developmental Biology, 2-2 Minatojima-Minamimachi, Chuo-ku, Kobe 650-0047, Japan. [3]Department of Molecular Medicine, Sapporo Medical University, S1 W17, Chuo-ku, Sapporo 060-8556, Japan. [4]Division of Experimental Immunology, Institute for Genome Research, University of Tokushima, 3-18-15 Kuramoto, Tokushima 770-8503, Japan. [5]Department of Pediatrics, Children's Hospital Medical Center, Division of Molecular Cardiovascular Biology, 3333 Burnet Avenue, Cincinnati, Ohio 45229-3039, USA. [6]Shanghai Institute of Cardiovascular Diseases, Zhongshan Hospital and Institutes of Biomedical Sciences, Fudan University, 180 Feng Lin Road, Shanghai 200032, China.
*These authors contributed equally to this work.

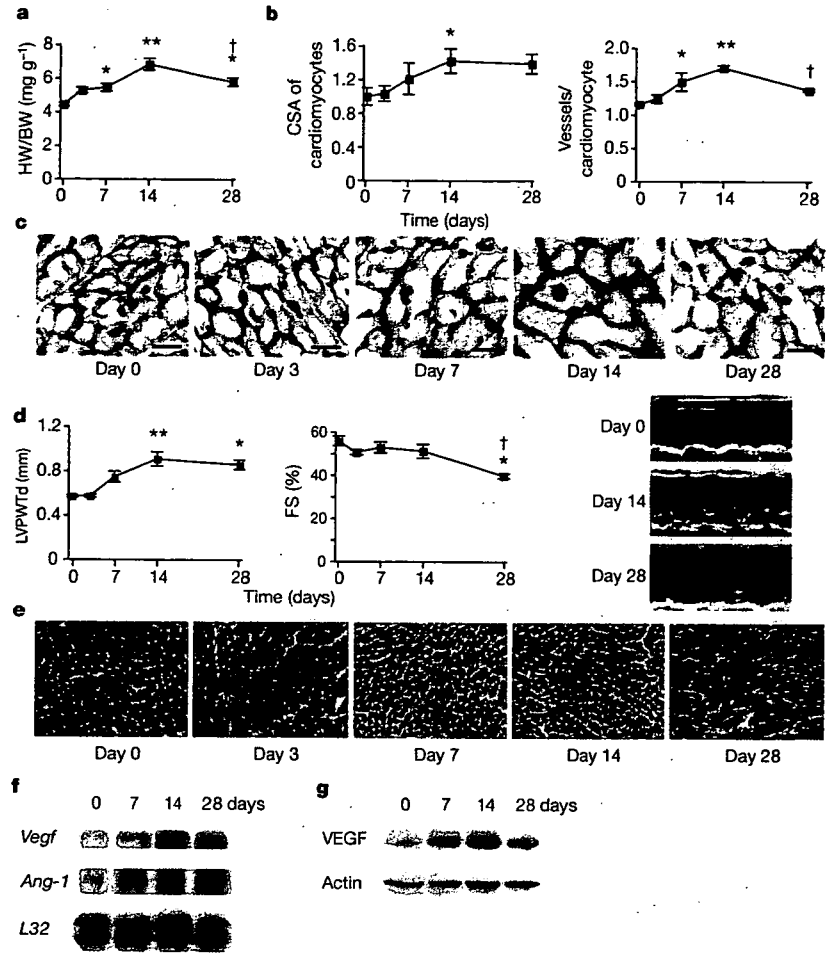

Figure 1 | Cardiac hypertrophy, function and angiogenesis after TAC. **a**, Heart weight/body weight (HW/BW) after TAC. **b**, Cross-sectional area (CSA) of cardiomyocytes and the number of microvessels per cardiomyocyte. **c**, Double-immunostaining for dystrophin (brown) and PECAM (black) of the TAC hearts. Scale bar, 20 μm. **d**, Echocardiographic analysis. FS, fractional shortening; LVPWTd, left ventricular posterior wall thickness. Asterisk, $P < 0.05$, two asterisks, $P < 0.001$ versus day 0; dagger, $P < 0.01$ versus day 14. Error bars indicate s.e.m.; $n = 7$ for **a**; $n = 3$ for **b**; $n = 5$ for **d**. **e**, Cardiac fibrosis. Scale bar, 50 μm. **f**, **g**, RNase protection assay (**f**) and western blot analysis (**g**) in the TAC heart.

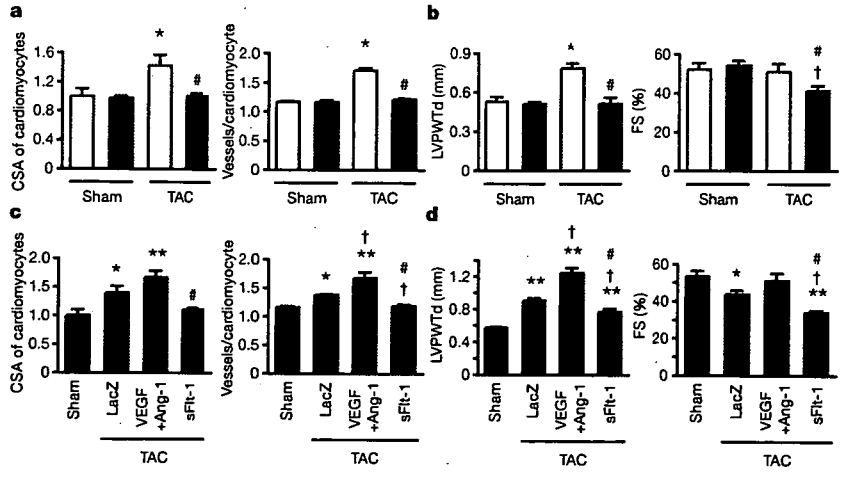

Figure 2 | Cardiac angiogenesis in TAC-induced hypertrophy. **a**, **b**, Mice were subjected to TAC or sham operation and treated with (filled columns) or without (open columns) TNP-470 for 2 weeks. Histological (**a**) and echocardiographic (**b**) analyses were performed. CSA, cross-sectional area; FS, fractional shortening; LVPWTd, left ventricular posterior wall thickness. Asterisk, $P < 0.005$ versus sham without TNP-470; dagger, $P < 0.01$ versus sham with TNP-470; hash sign, $P < 0.05$ versus TAC without TNP-470. Error bars indicate s.e.m.; $n = 3$ for **a**; $n = 5$ for **b**. **c**, **d**, Mice were infected with adenoviral vectors encoding VEGF and Ang-1, soluble Flt-1 (sFlt-1) or LacZ and subjected to 4 weeks of TAC or sham operation. Histological (**c**) and echocardiographic (**d**) analyses were performed. Asterisk, $P < 0.05$, two asterisks, $P < 0.005$ versus sham; dagger, $P < 0.05$ versus TAC with LacZ; hash sign, $P < 0.005$ versus TAC with VEGF + Ang-1. Error bars indicate s.e.m.; $n = 4$ for **c**; $n = 3$ for **d**.

factors, in the hearts of the TAC model. Expression of Hif-1α, but not that of Hif-2α, was increased by pressure overload from day 3 (Fig. 3a, and Supplementary Fig. 3a). Similarly, Hif-1 activity was increased from day 3 to day 14, indicating an important function for Hif-1α in the adaptive mechanism of cardiac hypertrophy (Fig. 3b, and Supplementary Fig. 4). To test this, we employed the conditional knockout mice in which the deletion of *Hif-1α* could be induced by tamoxifen only in cardiomyocytes (Supplementary Fig. 5a, b). Two weeks after TAC, both the expression of VEGF and the number of microvessels were significantly lower in the *Hif-1α* mutant mice than in control mice (Fig. 3c, d). Similarly, the development of cardiac hypertrophy was significantly attenuated in the *Hif-1α* mutant mice in comparison with control mice (Fig. 3d, e). Cardiac function in the *Hif-1α* mutant mice, but not in control mice, was significantly impaired at 2 weeks after TAC (Fig. 3e).

Our results indicate that the downregulation of Hif-1α and the resulting decreased angiogenic factors may cause maladaptive hypertrophy during chronic pressure overload. We next examined the extent of ischaemia in the hypertrophied myocardium with a hypoxyprobe[10]. Pressure overload induced cardiac hypoxia from as early as 3 days after TAC, and cardiac ischaemia was sustained until day 28 (Fig. 3f), indicating that a decrease in Hif-1α expression in the maladaptive phase was not due to an improvement of hypoxia in the myocardium by neoangiogenesis. It is generally accepted that Hif-1α is stabilized under mild or moderate hypoxia[11,12]. Prolonged or more severe hypoxia has been reported to induce the tumour suppressor p53, which binds to Hif-1α, promoting its degradation and inhibiting its transactivation properties[13,14]. We therefore examined whether p53 accumulates in the myocardium after chronic pressure overload, thereby inhibiting the Hif-1-dependent induction of angiogenic factors. Expression of p53 was markedly upregulated at 14 days after TAC, in accordance with an increase in atrial natriuretic factor (Anf), one of the markers for cardiac dysfunction (Fig. 3g, and Supplementary Fig. 4). Levels of phosphorylated p53 were also elevated in the maladaptive phase, whereas messenger RNA levels were unchanged (Fig. 3g, and Supplementary Fig. 3b). Chronic pressure overload increased the phosphorylation of Chk2, a protein kinase that mediates the p53-dependent DNA repair pathways (Fig. 3g). Expression of Bax, a pro-apoptotic factor regulated by p53, was also upregulated by sustained pressure overload (Fig. 3g), whereas

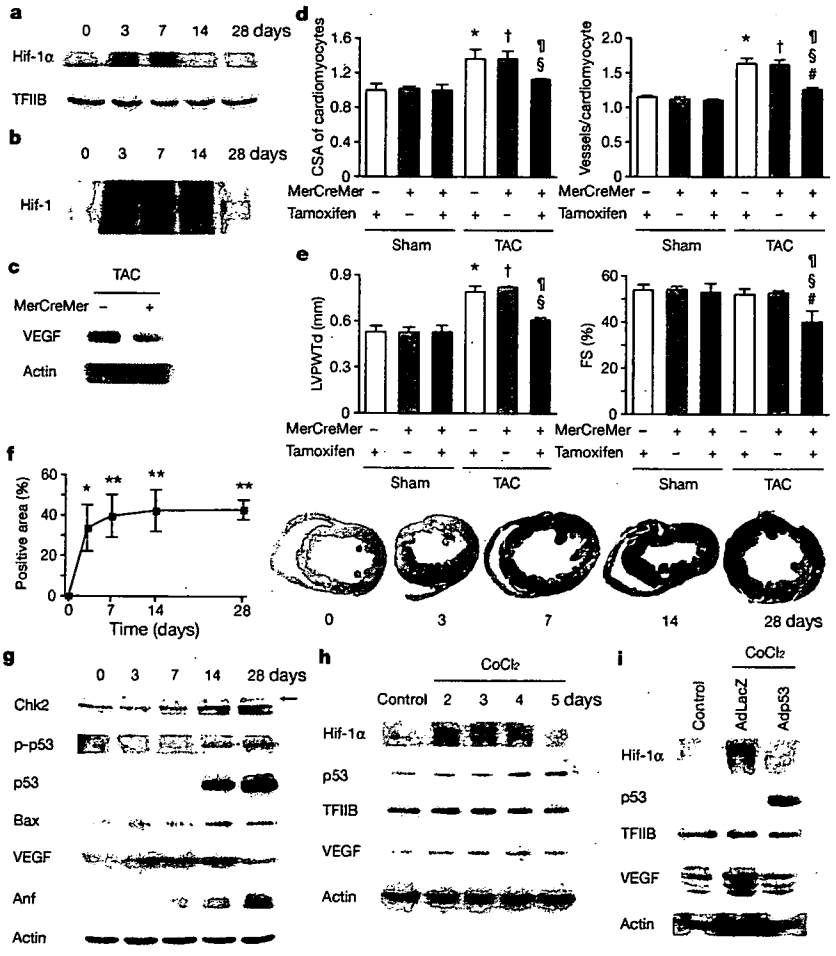

Figure 3 | Role of Hif-1 in adaptive hypertrophy. **a**, **b**, Hif-1α expression (**a**) and Hif-1 activity (**b**) in hearts during 4 weeks of TAC. **c**, Western blot analysis in the heart of mutant (+) or control (−) mice subjected to TAC and tamoxifen treatment. **d**, **e**, Histological (**d**) and echocardiographic (**e**) analyses of mutant mice (MerCreMer (+)/Tamoxifen (+)) or control littermates (MerCreMer (+)/Tamoxifen (−) or MerCreMer (−)/Tamoxifen (+)) subjected to 2 weeks of TAC or sham operation. CSA, cross-sectional area; FS, fractional shortening; LVPWTd, left ventricular posterior wall thickness. Asterisk, $P < 0.005$ versus sham/MerCreMer (−)/tamoxifen (+); dagger, $P < 0.005$ versus sham/MerCreMer (+)/tamoxifen (−); hash sign, $P < 0.05$ versus sham/MerCreMer (+)/tamoxifen (+); section sign, $P < 0.05$ versus TAC/MerCreMer (−)/tamoxifen (+); paragraph sign, $P < 0.05$ versus TAC/MerCreMer (+)/tamoxifen (−). Error bars indicate s.e.m.; $n = 4$. **f**, Cardiac ischaemia (brown). Asterisk, $P < 0.05$, two asterisks, $P < 0.01$ versus day 0. Error bars indicate s.e.m.; $n = 6$. **g**, Western blot analysis in hearts during 4 weeks of TAC. The arrow indicates the position of phospho-Chk2. **h**, Expression of Hif-1α, p53 and VEGF in primary cultured cardiomyocytes treated with $CoCl_2$. **i**, Expression of Hif-1α and p53 in cultured cardiomyocytes infected with an adenoviral vector encoding p53 (Adp53) or mock (AdLacZ) and treated with $CoCl_2$.

expression of anti-angiogenic factors such as thrombospondin-1 and plasminogen activator inhibitor-1 was unchanged (Supplementary Fig. 3c, d).

Treatment of cultured cardiomyocytes with $CoCl_2$, a hypoxia mimetic, induced the expression of Hif-1α and VEGF during days 2–4, but their expression was downregulated thereafter even in the presence of $CoCl_2$ (Fig. 3h). In contrast, p53 was increased at 4 days after treatment (Fig. 3h). Forced expression of p53 markedly inhibited the upregulation of Hif-1α and VEGF induced by $CoCl_2$ (Fig. 3i). Similar results were observed in cardiomyocytes exposed to hypoxia (Supplementary Fig. 6a, b). The introduction of p53 markedly attenuated Hif-1α expression, which was blocked by treatment with the proteasome inhibitor MG132 (Supplementary Fig. 6c). Hif-1α was co-immunoprecipitated with p53 in the presence of MG132 (Supplementary Fig. 6c). Treatment with $CoCl_2$ or hypoxia significantly upregulated the Hif-1 reporter activity (Supplementary Fig. 6d, e), and this upregulation was significantly suppressed by the introduction of p53 (Supplementary Fig. 6d, e), indicating a possibly crucial role of p53 in the downregulation of Hif-1α transcriptional activity.

To investigate the role of p53 in maladaptive hypertrophy, we produced the TAC model in p53-deficient mice. Cardiac Hif-1 activity and VEGF levels were higher in these mice at 4 weeks after TAC than in wild-type mice (Fig. 4a, b, and Supplementary Fig. 7). Consequently, the number of microvessels became significantly greater in the heart of p53-deficient mice than in wild-type mice 4 weeks after the operation (Fig. 4c). After chronic pressure overload, p53-deficient mice had more marked cardiac hypertrophy, better systolic function and lower Anf levels than wild-type mice (Fig. 4b, c, and Supplementary Fig. 7). Inhibition of p53 also has beneficial effects on cardiac function after myocardial infarction, and these effects may be partly attributable to increased neovascularization (Supplementary Fig. 8a–c).

We next used the p53 activator quinacrine[15] to examine whether p53 activation in the early phase of pressure overload promotes the transition of cardiac hypertrophy to heart failure. Administration of quinacrine significantly increased levels of p53 in the heart of sham-operated mice and enhanced the accumulation of p53 by TAC (Fig. 4d, and Supplementary Fig. 9). The induction of Hif-1 activity and VEGF expression by TAC was significantly suppressed in the heart of quinacrine-treated mice (Fig. 4d, e, and Supplementary Fig. 9). Consequently, p53 upregulated by quinacrine treatment severely impaired cardiac angiogenesis induced by TAC and attenuated adaptive hypertrophy, leading to systolic dysfunction associated with increased Anf levels at 2 weeks after the operation (Fig. 4d, f, and Supplementary Fig. 9). These effects of quinacrine were blunted in p53-deficient mice (Supplementary Fig. 10a, b). The number of cardiomyocytes positive for TdT-mediated dUTP nick end labelling

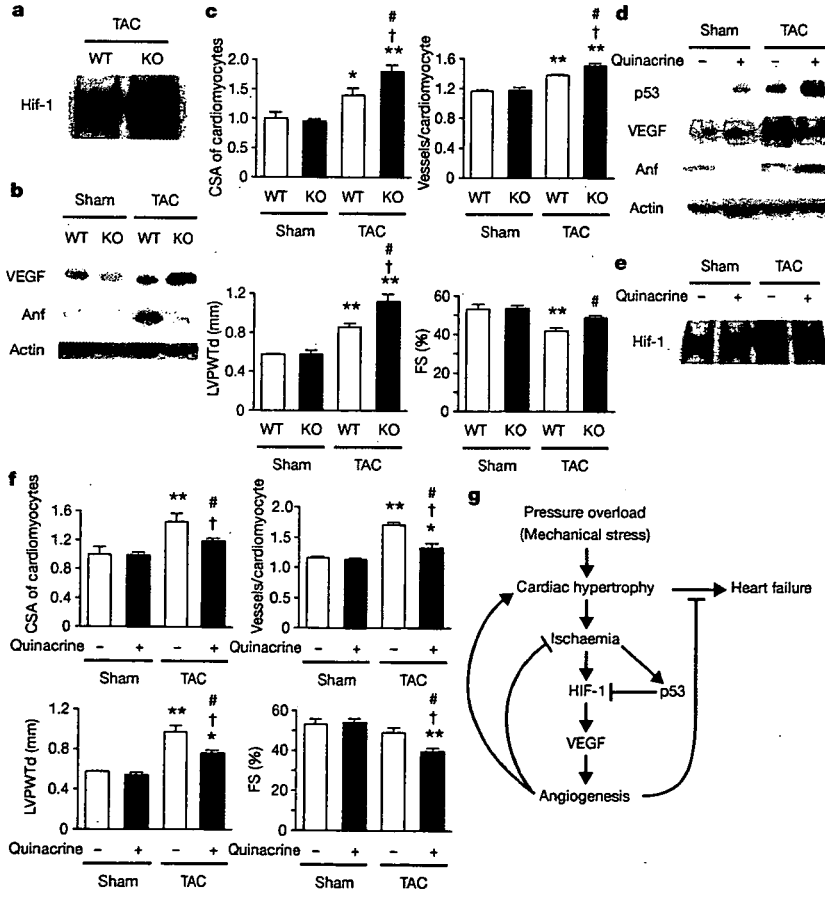

Figure 4 | Role of p53 accumulation in maladaptive hypertrophy. **a–c**, Wild-type (WT) and p53-deficient mice (KO) were subjected to 4 weeks of TAC or sham operation. Gel mobility-shift assay (**a**), western blotting (**b**) and histological and echocardiographic analyses (**c**) were performed. CSA, cross-sectional area; FS, fractional shortening; LVPWTd, left ventricular posterior wall thickness. Asterisk, $P < 0.05$, two asterisks, $P < 0.005$ versus wild-type sham; dagger, $P < 0.001$ versus KO sham; hash sign, $P < 0.05$ versus wild-type TAC. Error bars indicate s.e.m.; $n = 4$. **d–f**, Wild-type mice were treated with quinacrine (+) or vehicle (−) and subjected to 2 weeks of TAC or sham operation. Western blot analysis (**d**), gel mobility-shift assay (**e**) and histological and echocardiographic analyses (**f**) were performed. Asterisk, $P < 0.05$, two asterisks, $P < 0.005$ versus vehicle sham; dagger, $P < 0.05$ versus quinacrine sham; hash sign, $P < 0.05$ versus vehicle TAC. Error bars indicate s.e.m.; $n = 4$. **g**, Proposed mechanism underlying the transition from cardiac hypertrophy to heart failure.

(TUNEL) was significantly increased in the late phase of pressure overload, and this increase was attenuated by p53 deficiency (Supplementary Fig. 11a). Treatment with quinacrine increased the expression of p53 in both cardiomyocytes and endothelial cells but did not decrease the viability of these cells, microvessel density or cardiac function, in sham-operated mice (Fig. 4d, f, and Supplementary Figs 9 and 11b, c). In contrast, the number of TUNEL-positive endothelial cells and cardiomyocytes was significantly increased in the TAC heart treated with quinacrine (Supplementary Fig. 11b), which was associated with an increase in Bax expression (Supplementary Fig. 11c). Although p53-inducible pro-apoptotic genes have been implicated in hypoxia-mediated cell death[16,17], these results indicate that upregulated p53 may not cause cardiomyocyte death or systolic dysfunction directly but does so indirectly through the inhibition of cardiac angiogenesis.

Our results show that p53 is a crucial regulator in the induction of maladaptive hypertrophy, and that it does so by inhibiting cardiac angiogenesis (Fig. 4g). Gene therapy with constitutively active HIF-1α, which is resistant to degradation under normoxia, is currently being examined in clinical trials for peripheral vascular disease[18,19] and may be effective for the treatment of heart failure induced by pressure overload. Although further studies are required, inhibition of p53 or promotion of vascular growth in the heart may be a novel therapeutic strategy for preventing the transition from cardiac hypertrophy to heart failure. This strategy may be also useful to improve systolic dysfunction caused by various stimuli that increase cardiac p53 activity[20].

METHODS

Animal models. All protocols were approved by Chiba University review board. TAC was performed as described previously[21] on 8-week-old male C57BL/6 mice (SLC).

Physiological analysis and histological analysis. Echocardiography was performed as described previously[22]. Frozen cross-sections of heart samples were stained with antibodies against specific proteins as described in Supplementary Information.

Conditional ablation of the *Hif-1α* gene in cardiomyocytes of adult murine heart. We prepared transgenic mice in which a transgene encoding Cre recombinase fused to the mutated oestrogen receptor domains (MerCreMer) was driven by the cardiomyocyte-specific α-myosin heavy chain (MHC) promoter[23]. We then crossed the MHC-MerCreMer mice with mice that carried floxed *Hif-1α* alleles ($Hif\text{-}1\alpha^{floxed/floxed}$)[24] and produced MHC-MerCreMer;$Hif\text{-}1\alpha^{floxed/floxed}$ mutant mice.

Western blot analysis. Whole-cell lysates (30–50 μg) or nuclear extracts (10–20 μg) were resolved by SDS–polyacrylamide gel electrophoresis. Proteins were transferred to a polyvinylidene difluoride membrane (Millipore) and incubated with the first antibody followed by an anti-immunoglobulin-G–horseradish peroxidase antibody (Jackson ImmunoResearch). Specific proteins were detected by enhanced chemiluminescence (Amersham).

Statistical analysis. Data are shown as means ± s.e.m. Multiple group comparison was performed by one-way analysis of variance followed by the Bonferroni procedure for comparison of means.

Received 1 November 2006; accepted 15 January 2007.
Published online 4 March 2007.

1. Frey, N. & Olson, E. N. Cardiac hypertrophy: the good, the bad, and the ugly. *Annu. Rev. Physiol.* 65, 45–79 (2003).
2. Levy, D. *et al.* Prognostic implications of echocardiographically determined left ventricular mass in the Framingham Heart Study. *N. Engl. J. Med.* 322, 1561–1566 (1990).
3. Marcus, M. L. *et al.* Abnormalities in the coronary circulation that occur as a consequence of cardiac hypertrophy. *Am. J. Med.* 75, 62–66 (1983).
4. Tomanek, R. J. Response of the coronary vasculature to myocardial hypertrophy. *J. Am. Coll. Cardiol.* 15, 528–533 (1990).
5. Giordano, F. J. *et al.* A cardiac myocyte vascular endothelial growth factor paracrine pathway is required to maintain cardiac function. *Proc. Natl Acad. Sci. USA* 98, 5780–5785 (2001).
6. Shyu, K. G. *et al.* Carvedilol prevents cardiac hypertrophy and overexpression of hypoxia-inducible factor-1α and vascular endothelial growth factor in pressure-overloaded rat heart. *J. Biomed. Sci.* 12, 409–420 (2005).
7. Yoon, Y. S. *et al.* Progressive attenuation of myocardial vascular endothelial growth factor expression is a seminal event in diabetic cardiomyopathy: restoration of microvascular homeostasis and recovery of cardiac function in diabetic cardiomyopathy after replenishment of local vascular endothelial growth factor. *Circulation* 111, 2073–2085 (2005).
8. Ingber, D. *et al.* Synthetic analogues of fumagillin that inhibit angiogenesis and suppress tumour growth. *Nature* 348, 555–557 (1990).
9. Goldman, C. K. *et al.* Paracrine expression of a native soluble vascular endothelial growth factor receptor inhibits tumor growth, metastasis, and mortality rate. *Proc. Natl Acad. Sci. USA* 95, 8795–8800 (1998).
10. Morani, A. *et al.* Lung dysfunction causes systemic hypoxia in estrogen receptor β knockout ($ER\beta^{-/-}$) mice. *Proc. Natl Acad. Sci. USA* 103, 7165–7169 (2006).
11. Semenza, G. L. Targeting HIF-1 for cancer therapy. *Nature Rev. Cancer* 3, 721–732 (2003).
12. Pugh, C. W. & Ratcliffe, P. J. Regulation of angiogenesis by hypoxia: role of the HIF system. *Nature Med.* 9, 677–684 (2003).
13. Blagosklonny, M. V. *et al.* p53 inhibits hypoxia-inducible factor-stimulated transcription. *J. Biol. Chem.* 273, 11995–11998 (1998).
14. Ravi, R. *et al.* Regulation of tumor angiogenesis by p53-induced degradation of hypoxia-inducible factor 1α. *Genes Dev.* 14, 34–44 (2000).
15. Gurova, K. V. *et al.* Small molecules that reactivate p53 in renal cell carcinoma reveal a NF-κB-dependent mechanism of p53 suppression in tumors. *Proc. Natl Acad. Sci. USA* 102, 17448–17453 (2005).
16. Fei, P. *et al.* Bnip3L is induced by p53 under hypoxia, and its knockdown promotes tumor growth. *Cancer Cell* 6, 597–609 (2004).
17. Kubasiak, L. A., Hernandez, O. M., Bishopric, N. H. & Webster, K. A. Hypoxia and acidosis activate cardiac myocyte death through the Bcl-2 family protein BNIP3. *Proc. Natl Acad. Sci. USA* 99, 12825–12830 (2002).
18. Kelly, B. D. *et al.* Cell type-specific regulation of angiogenic growth factor gene expression and induction of angiogenesis in nonischemic tissue by a constitutively active form of hypoxia-inducible factor 1. *Circ. Res.* 93, 1074–1081 (2003).
19. Patel, T. H. *et al.* Constitutively active HIF-1α improves perfusion and arterial remodeling in an endovascular model of limb ischemia. *Cardiovasc. Res.* 68, 144–154 (2005).
20. Shizukuda, Y. *et al.* Targeted disruption of p53 attenuates doxorubicin-induced cardiac toxicity in mice. *Mol. Cell. Biochem.* 273, 25–32 (2005).
21. Takimoto, E. *et al.* Sodium calcium exchanger plays a key role in alteration of cardiac function in response to pressure overload. *FASEB J.* 16, 373–378 (2002).
22. Harada, M. *et al.* G-CSF prevents cardiac remodeling after myocardial infarction by activating the Jak-Stat pathway in cardiomyocytes. *Nature Med.* 11, 305–311 (2005).
23. Sohal, D. S. *et al.* Temporally regulated and tissue-specific gene manipulations in the adult and embryonic heart using a tamoxifen-inducible Cre protein. *Circ. Res.* 89, 20–25 (2001).
24. Tomita, S. *et al.* Defective brain development in mice lacking the Hif-1α gene in neural cells. *Mol. Cell. Biol.* 23, 6739–6749 (2003).

Supplementary Information is linked to the online version of the paper at www.nature.com/nature.

Acknowledgements We thank E. Fujita, R. Kobayashi and M. Ikeda for technical support. This work was supported by a Grant-in-Aid for Scientific Research on Priority Areas and for Exploratory Research, Ministry of Education, Culture, Sports, Science and Technology; Health and Labour Sciences Research Grants; Research on Measures for Intractable Diseases; Grants from Goho Life Sciences International Fund; an Academic Award of the Mochida Memorial Foundation and Uehara Memorial Foundation (to I.K.); and grants from the Suzuken Memorial Foundation, the NOVARTIS Foundation and the Ministry of Education, Culture, Sports, Science and Technology of Japan (to T.M.).

Author Contributions M.S., T.M., H.T., H.M., M.O., Y.Q., H.A., K.T., Y.K., M.H., I.S. and Y.Z. performed the experiments. T.A., H.H., S.T. and J.D.M. provided reagents or mice. M.S., T.M. and I.K. designed and prepared the manuscript. I.K. planned and supervised the project.

Author Information Reprints and permissions information is available at www.nature.com/reprints. The authors declare no competing financial interests. Correspondence and requests for materials should be addressed to I.K. (komuro-tky@umin.ac.jp).

UTF1 is a chromatin-associated protein involved in ES cell differentiation

Vincent van den Boom,[1] Susanne M. Kooistra,[1] Marije Boesjes,[1] Bart Geverts,[2] Adriaan B. Houtsmuller,[2] Koshiro Monzen,[5] Issei Komuro,[6] Jeroen Essers,[3,4] Loes J. Drenth-Diephuis,[1] and Bart J.L. Eggen[1]

[1]Developmental Genetics, Groningen Biomolecular Sciences and Biotechnology Institute, University of Groningen, 9750 AA Haren, Netherlands
[2]Department of Pathology, [3]Department of Cell Biology and Genetics, and [4]Department of Radiation Oncology, Erasmus MC, 3000 CA Rotterdam, Netherlands
[5]Department of Cardiovascular Medicine, University of Tokyo Graduate School of Medicine, Bunkyo-ku, Tokyo 113-8655, Japan
[6]Department of Cardiovascular Science and Medicine, Chiba University Graduate School of Medicine, Chuo-ku, Chiba 260-8670, Japan

Embryonic stem (ES) cells are able to grow indefinitely (self-renewal) and have the potential to differentiate into all adult cell types (pluripotency). The regulatory network that controls pluripotency is well characterized, whereas the molecular basis for the transition from self-renewal to the differentiation of ES cells is much less understood, although dynamic epigenetic gene silencing and chromatin compaction are clearly implicated. In this study, we report that UTF1 (undifferentiated embryonic cell transcription factor 1) is involved in ES cell differentiation. Knockdown of UTF1 in ES and carcinoma cells resulted in a substantial delay or block in differentiation. Further analysis using fluorescence recovery after photobleaching assays, subnuclear fractionations, and reporter assays revealed that UTF1 is a stably chromatin-associated transcriptional repressor protein with a dynamic behavior similar to core histones. An N-terminal Myb/SANT domain and a C-terminal domain containing a putative leucine zipper are required for these properties of UTF1. These data demonstrate that UTF1 is a strongly chromatin-associated protein involved in the initiation of ES cell differentiation.

Introduction

Mouse embryonic stem (ES) cells derived from the inner cell mass of blastocyst embryos have the ability to self-renew and are pluripotent. ES cell pluripotency is maintained via the LIF-gp130-STAT3, bone morphogenetic protein (BMP)–Smad-Id, and probably Wnt and mTOR signaling cascades (Smith et al., 1988; Williams et al., 1988; Niwa et al., 1998; Matsuda et al., 1999; Ying et al., 2003; Gangloff et al., 2004; Murakami et al., 2004; Sato et al., 2004). Intracellular regulators of ES cell self-renewal include Oct4, Sox2, Nanog, and the recently implicated transcription factors Sall4, Esrrb, Tbx3, and Tcl1 (Yuan et al., 1995; Nichols et al., 1998; Niwa et al., 2002; Chambers et al., 2003; Mitsui et al., 2003; Ivanova et al., 2006; Zhang et al., 2006).

Using chromatin immunoprecipitation on chip analyses to map Oct4, Sox2, and Nanog target genes, a large group of genes was identified that is coregulated by these factors in different combinations, although the majority of genes was cooccupied by Oct4, Sox2, and Nanog (Boyer et al., 2005; Loh et al., 2006). Interestingly, many of these target genes are not expressed in ES cells.

Recent reports showed that in ES cells, many differentiation genes are silenced by Polycomb group (PcG) complexes, indicating that the epigenetic regulation of gene expression is essential for maintaining ES cell pluripotency (Azuara et al., 2006; Bernstein et al., 2006; Boyer et al., 2006; Bracken et al., 2006; Lee et al., 2006; Loh et al., 2006). Interestingly, many of the repressed Nanog, Oct4, and Sox2 target genes were cooccupied by PcG complexes, suggesting that ES cells are poised to enter differentiation programs but are held in check by PcG-mediated chromatin modifications. The suggestion that epigenetic regulation is an important instrument to control ES cell pluripotency versus their capacity to differentiate is further supported by the findings that the PcG protein Suz12 is required for ES cell differentiation (Pasini et al., 2007) and that a functional NuRD (nucleosome remodeling and disruption) complex, which is involved in nucleosome remodeling, is required for the lineage commitment of ES cells (Kaji et al., 2006).

V. van den Boom and S.M. Kooistra contributed equally to this paper.

Correspondence to Bart J.L. Eggen: b.j.l.eggen@rug.nl

V. van den Boom's present address is Department of Cell Biology, Section of Stem Cell Biology, University Medical Centre Groningen, 9700 RB Groningen, Netherlands.

Abbreviations used in this paper: BMP, bone morphogenetic protein; BRE, BMP-responsive element; CD, conserved domain; EB, embryoid body; EC, embryonic carcinoma; eGFP, enhanced GFP; ES, embryonic stem; HDAC1, histone deacetylase 1; KD, knockdown; mUTF1, mouse UTF1; PcG, Polycomb group; SBE, Smad-binding element; TK, thymidine kinase; UTF1, undifferentiated embryonic cell transcription factor 1; wt, wild type.

The online version of this article contains supplemental material.

The Journal of Cell Biology, Vol. 178, No. 6, September 10, 2007 913–924
http://www.jcb.org/cgi/doi/10.1083/jcb.200702058

Supplemental Material can be found at:
http://www.jcb.org/cgi/content/full/jcb.200702058/DC1

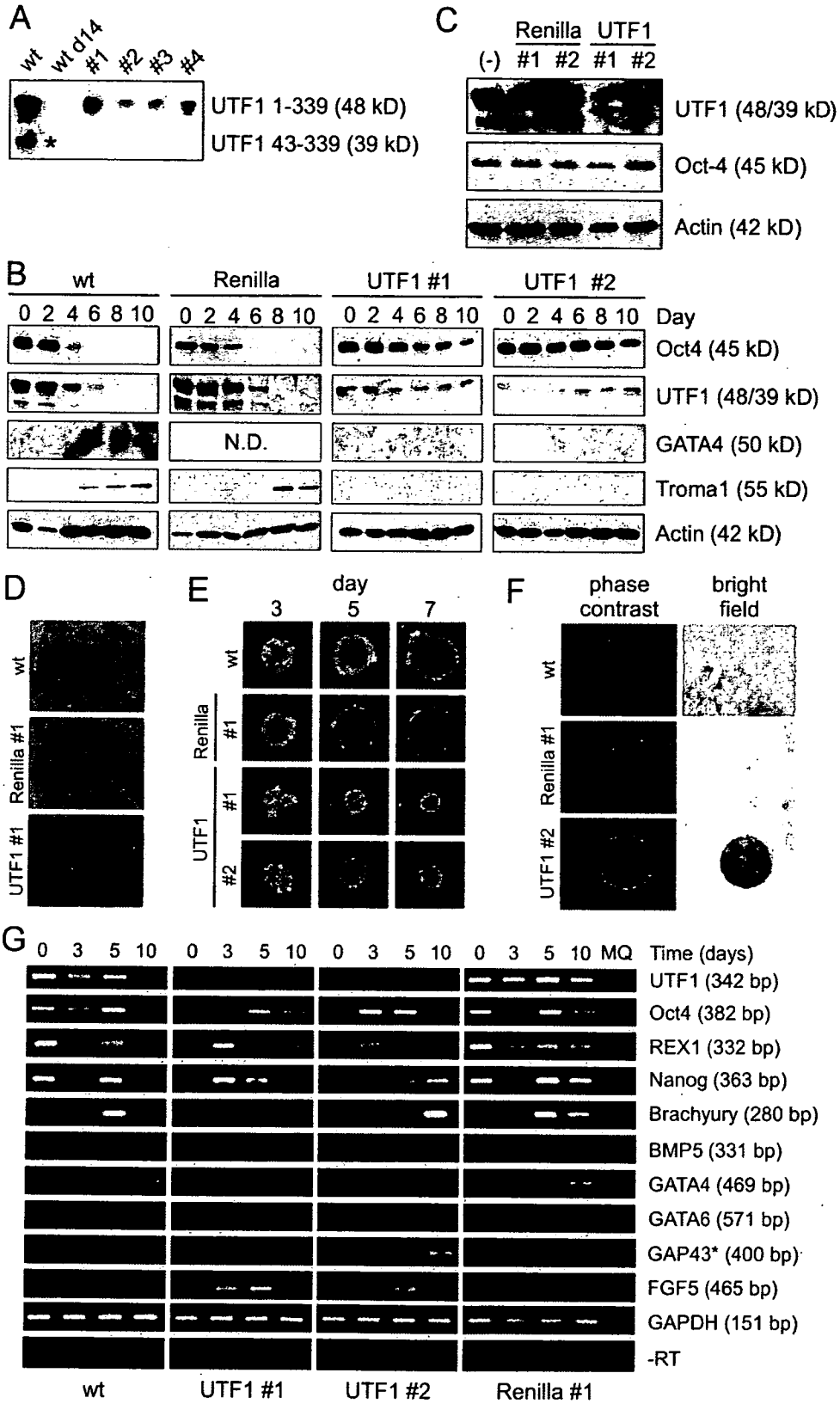

Apart from *Oct4*, *Sox2*, and *Nanog*, other genes are also highly and almost exclusively expressed during early embryogenesis (Mitsui et al., 2003; Ivanova et al., 2006). One of these genes, the *UTF1* (*undifferentiated embryonic cell transcription factor 1*) gene, is specifically expressed in the inner cell mass and primitive ectoderm and is down-regulated at early primitive streak stages (Okuda et al., 1998). Expression is maintained in the primordial germ cells in developing embryos and in the gonads in adult animals (Chuva de Sousa Lopes et al., 2005). Promoter analysis indicated that the murine *UTF1* gene is transcriptionally regulated by Oct4 and Sox2 (Nishimoto et al., 1999). The UTF1 protein was shown to repress transcription (Fukushima et al., 1999), to activate reporter genes in an ATF2-dependent manner, and to interact with the basal transcription factor TFIID (Fukushima et al., 1998; Okuda et al., 1998). A recent study suggested a role for UTF1 in the proliferation rate and teratoma-forming capacity of ES cells (Nishimoto et al., 2005).

The purpose of this study was to determine the requirement of UTF1 for ES cell self-renewal and/or differentiation and to gain insight into its mechanistic properties. Using knockdown (KD) strategies, we determined that UTF1 is involved in ES cell differentiation. UTF1 KD perturbed ES and embryonic carcinoma (EC) cell differentiation, whereas their ability to self-renew was unaffected. UTF1 displays transcriptional repressor activity, and a combination of localization experiments, FRAP protocols, and subcellular fractionation assays indicated that UTF1 is stably chromatin associated with dynamics and biochemical properties similar to core histones.

Results

UTF1 is required for EC cell differentiation

To study the potential role of mouse UTF1 (mUTF1; hereafter UTF1) in ES and EC cell differentiation, we stably expressed UTF1 and Renilla luciferase (hereafter Renilla) siRNAs in P19CL6 EC cells. UTF1 expression levels were substantially decreased in all clones tested (Fig. 1 A), whereas expression levels of the pluripotency marker Oct4 were not affected (Fig. 1 B). Next, DMSO-induced differentiation of wild-type (wt), Renilla, and UTF1 KD cells was analyzed (Fig. 1 B). wt and Renilla KD cells differentiated normally, which was reflected by a drastic reduction in Oct4 levels around day 4, decreased UTF1 levels between days 4 and 6, and detectable GATA4 (not determined for Renilla) and Troma1 expression by day 8. Actin was used as a protein loading control. In UTF1 KD lines, the differentiation-induced down-regulation of Oct4 was either delayed (#1) or minor (#2), and both GATA4 and Troma1 were not detected. Residual UTF1 protein levels were not further down-regulated, most likely as a consequence of high Oct4 levels, a transcriptional activator of the *UTF1* gene.

As UTF1 was previously reported to be involved in ES cell proliferation (Nishimoto et al., 2005), we determined the doubling times of wt, Renilla KD, and UTF1 KD EC cells. UTF1 KD cells showed a 24% and 17% increase in doubling time (8.9 ± 0.3 h) compared with wt EC (7.2 ± 0.1 h) and Renilla KD (7.6 ± 0.3 h) cells, respectively. Next, the differentiation of wt and UTF1 KD EC cells was performed with different cell numbers to rule out potential cell density effects on differentiation (0.5 and 2 times the number of cells: 1.8×10^5 and 7.3×10^5 cells, respectively). Irrespective of the initial number of cells, the differentiation of UTF1 KD cells was always delayed or blocked, whereas wt cells differentiated normally (unpublished data). Summarizing, these data indicate that in EC cells, UTF1 KD results in an abrogated differentiation capacity and persistent Oct4 expression under differentiation-inducing conditions.

UTF1 is involved in ES cell differentiation

To extend these findings to a nontransformed mouse cell line, we tested the effect of UTF1 KD on IB10 ES cell differentiation. Renilla KD clones expressed normal levels of UTF1 and Oct4, whereas in UTF1 KD cell lines, UTF1 levels were reduced, but Oct4 expression was not affected (Fig. 1 C). In addition, UTF1 and Renilla KD ES cells are positive for AP, confirming their ES cell phenotype (Fig. 1 D). To determine whether UTF1 down-regulation also affected the differentiation potential of these cells, embryoid bodies (EBs) were generated. Where wt and Renilla KD cells formed normal EBs with high efficiency, UTF1 KD–derived EBs were irregularly shaped, much smaller in size, formed with low efficiency, and compaction was not observed (Fig. 1 E).

In agreement with observations by Nishimoto et al. (2005), UTF1 KD affected (although less dramatically) the doubling time of ES cells: UTF1 KD ES cells have a doubling time of 11.8 ± 0.7 h compared with 9.6 ± 0.7 h and 10.2 ± 0.1 h for wt (23% increase) and Renilla (16% increase) ES cells, respectively. Because UTF1 KD abrogated the ability of EC cells to differentiate, we tested whether EBs from UTF1 KD ES cells

Figure 1. **UTF1 is involved in the differentiation of EC and ES cells.** (A) UTF1 expression in P19CL6 EC cells (wt), 14-d DMSO-differentiated EC cells (wt d14), and four independent UTF1 EC KD clones (UTF1 #1–#4). The asterisk indicates a shorter variant of mUTF1 (aa 43–339) generated by transcription from an alternative start site (Nishimoto et al., 2001). (B) DMSO-induced differentiation of wt, Renilla luciferase KD (Renilla), and UTF1 KD (UTF1 #1 and #2) EC cells. Cell lysates were analyzed with antibodies against Oct4, UTF1, GATA4, and Troma1. Actin staining was performed as a loading control. (C) Western analysis of wt, Renilla luciferase KD (Renilla #1 and #2), and UTF1 KD (UTF1 #1 and #2) IB10 ES cells. Cell lysates were analyzed with antibodies against UTF1 and Oct4. Actin levels were determined to correct for gel loading. (D) Brightfield images of wt, Renilla luciferase KD (Renilla #1), and UTF1 KD (UTF1 #1) ES cells stained for AP activity. (E) Phase-contrast images of EBs from wt, Renilla luciferase KD (Renilla #1), and UTF1 KD (UTF1 #1 and #2) ES cells after 3, 5, and 7 d. (F) Phase-contrast and brightfield images of day 8 EBs from wt, Renilla luciferase KD (Renilla #1), and UTF1 KD (UTF1 #2) ES cells stained for AP activity. (G) Expression levels of markers for ES cells (*UTF1*, *Oct4*, *REX1*, and *Nanog*), ectoderm (FGF5 and GAP43), mesoderm (*Brachyury* and *BMP5*), and endoderm (*GATA4* and *GATA6*) were measured by semiquantitative RT-PCR in undifferentiated ES cells and EBs cultured for 3, 5, and 10 d. *Glyceraldehyde-3-phosphate dehydrogenase* (*GAPDH*) expression was used as a control. In the −RT lanes, reverse transcriptase was omitted from the reverse transcriptase reactions to control for genomic DNA contamination and amplified using *glyceraldehyde-3-phosphate dehydrogenase* primers. A representative experiment is depicted. The asterisk indicates that the 5- and 10-d GAP43 RT-PCR products were not loaded in adjacent lanes. Bars, 250 μm.

also failed to differentiate. AP staining showed that day 8 wt and Renilla EBs are largely AP negative, whereas UTF1 KD EBs still displayed substantial AP activity, suggesting that UTF1 is involved in ES cell differentiation (Fig. 1 F). To further validate this observation, the expression pattern of several germ layer–specific marker genes during EB development was determined by RT-PCR (Fig. 1 G). Both wt and Renilla ES cells show a clear up-regulation of various lineage markers. At days 3–5, Brachyury (early mesoderm) was detected, and at day 10, BMP5 (dorsal mesoderm) was detected. Endoderm markers GATA4 and GATA6 were detected at day 10, and ectoderm markers GAP43 and FGF5 were both detected at days 3–10. In contrast, both UTF1 KD cell lines showed either an absence (GATA6), minor (GATA4 and BMP5), or delayed (Brachyury) expression of these markers. However, ectoderm markers FGF5 and GAP43 were detected from day 3. Pluripotency markers like Oct4, REX1, and Nanog were detected at all time points in the various EBs, most likely as a result of the incomplete differentiation of a subset of cells.

The increased doubling time of UTF1 KD ES cells could (partially) be responsible for the observed differentiation defect. However, already after 48 h, when differences in doubling times have not yet resulted in substantial differences in cell numbers, we observed that UTF1 KD cells often failed to form aggregates (unpublished data). This strongly suggests that the observed effects on EB formation and differentiation cannot solely be explained by the increased doubling time of UTF1 KD cells. Collectively, these data show that UTF1 KD in ES cells results in perturbed EB formation and a severely reduced differentiation potential in the endodermal and mesodermal lineages.

UTF1 is a chromatin-associated transcriptional repressor

To understand the mechanistic properties of UTF1 that underlie its involvement in EC and ES cell differentiation, a series of experiments were performed to molecularly characterize the protein. First, we determined the subcellular localization of UTF1

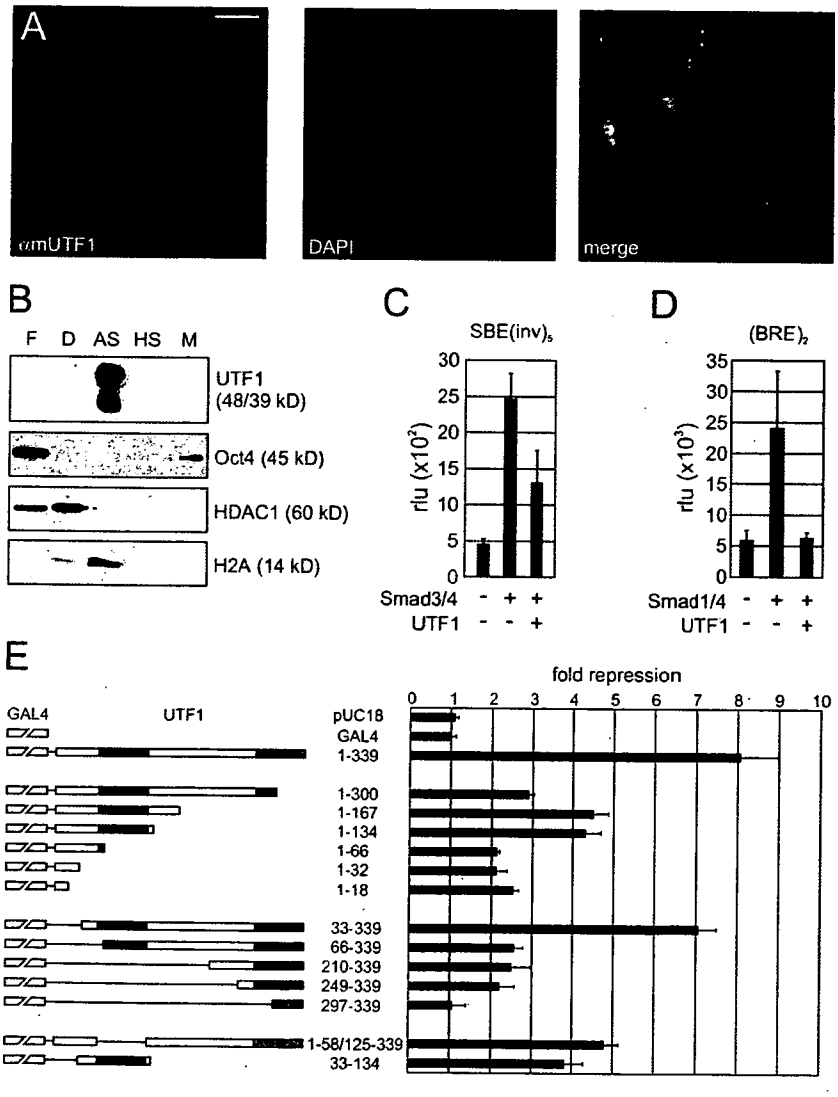

Figure 2. **Characterization of localization, fractionation, and reporter activity of UTF1.** (A) Immunofluorescence analysis of endogenous UTF1 in EC cells using an antibody directed against UTF1. (B) Subnuclear fractionation of EC cells: F, free-diffusing protein fraction; D, DNaseI fraction; AS, ammonium sulfate fraction; HS, high salt fraction; M, nuclear matrix fraction. Fractions were immunostained with antibodies recognizing UTF1, Oct4, HDAC1, and histone H2A. (C and D) Reporter analysis of HepG2 cells transfected with the $SBE(inv)_5$ reporter, $(BRE)_2$ reporter, Smad 3/4, Smad 1/4, and UTF1 as indicated. In all transfections, a LacZ expression plasmid, pDM2-LacZ, was included as an internal standard, and relative luciferase units (rlu) are depicted as the mean with SD (error bars). In all samples, equal amounts of expression plasmids were present by the addition of empty pcDNA3 plasmid when required. (E) Mapping the UTF1 repressor domains. A schematic representation of GAL4-UTF1 constructs used in this experiment; the Myb/SANT domain and CD2 are represented by black boxes and gray boxes, respectively. Different GAL4-UTF1 constructs and a constitutive active TK-luciferase reporter containing five GAL4-binding sites (UAS-TK-Luc) were transfected into HepG2 cells. The inhibitory effect of UTF1 on reporter activity is depicted as fold repression compared with GAL4 alone. In all transfections, a LacZ expression plasmid, pDM2-LacZ, was included as an internal standard, and normalized luciferase activity is depicted as the mean with SD. Bar, 15 μm.

in EC cells (Fig. 2 A). UTF1 was clearly localized to the nucleus and excluded from the nucleoli. In addition, we found UTF1 to localize to the chromosomes at different stages during cell division. To further characterize this potential interaction between UTF1 and the DNA/chromatin, we performed subnuclear fractionations of EC cells separating free-diffusing proteins (cytosolic and nuclear), weak/strong DNA-associated proteins, and nuclear matrix (associated) proteins. UTF1 is observed exclusively in the ammonium sulfate fraction known to contain strongly DNA-associated proteins, like core histone H2A (Fig. 2 B). In contrast, Oct4 primarily localized to the free-diffusing fraction and, to some extent, to the nuclear matrix fraction, indicating that Oct4 and UTF1 have distinct chromatin-binding characteristics. To compare the observed behavior of UTF1 to that of chromatin-modifying proteins, we determined the fractions containing histone deacetylase 1 (HDAC1; Fig. 2 B). Unlike UTF1, HDAC1 is found in the fractions containing free-diffusing and weak DNA-associated proteins. Collectively, these data suggest that UTF1 is a protein with a high affinity for chromatin, similar to that of core histones and different from chromatin-modifying proteins like HDAC1.

As a chromatin-associated protein, UTF1 is likely to be involved in gene expression regulation. To determine the effect of UTF1 on promoter activity, reporter assays were performed using constructs containing multiple copies of either the Smad-binding element (SBE) or BMP-responsive element (BRE). These reporters were used because we previously identified UTF1 as an SBE-interacting protein in a yeast 1 hybrid screen. However, more detailed analysis showed that UTF1 is not specifically involved in Smad signaling. The reporters are activated

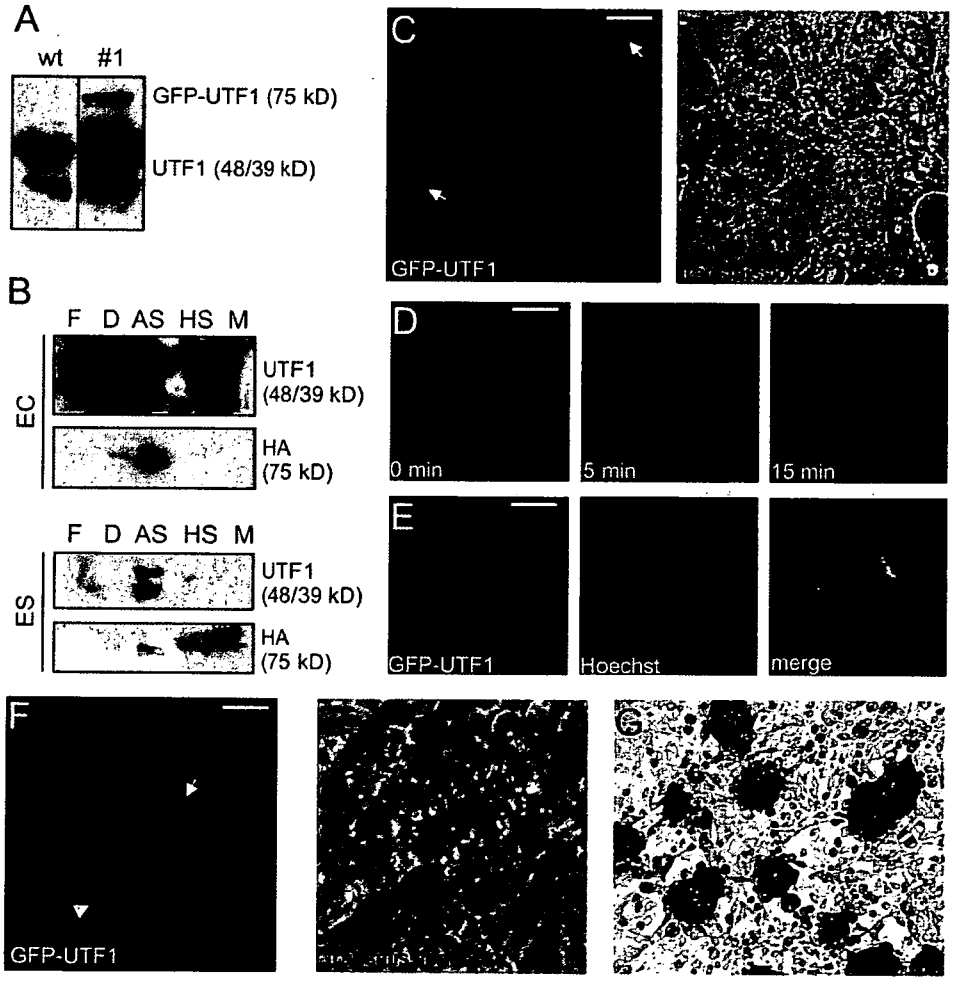

Figure 3. **Cellular localization and subnuclear fractionation of GFP-UTF1 in EC and ES cells.** (A) Western blot analysis of wild type (wt) EC cells and a clone stably expressing GFP-UTF1 (#1) using an antibody directed against UTF1. (B) Subnuclear fractionation of EC and ES cells, both expressing GFP-UTF1. Immunoblot analysis was performed with an antibody directed against UTF1 and the HA tag of the fusion protein. F, free-diffusing protein fraction; D, DNaseI fraction; AS, ammonium sulfate fraction; HS, high salt fraction; M, nuclear matrix fraction. (C) Confocal and transmission image of living EC cells expressing GFP-UTF1. Nucleoli are indicated by arrows. (D) Time-lapse imaging of a GFP-UTF1–expressing EC cell going through mitosis. (E) Confocal images of a mitotic GFP-UTF1–expressing cell treated with Hoechst. (F) Confocal and transmission images of GFP-UTF1–expressing ES cells grown on an STO cell feeder layer. The arrow indicates a nucleolus, and the arrowhead points to mitoticchromosomes. (G) Transmission image of AP staining of GFP-UTF1 ES cells. The underlying STO feeder cells are negative for AP activity. Bars, 15 μm.

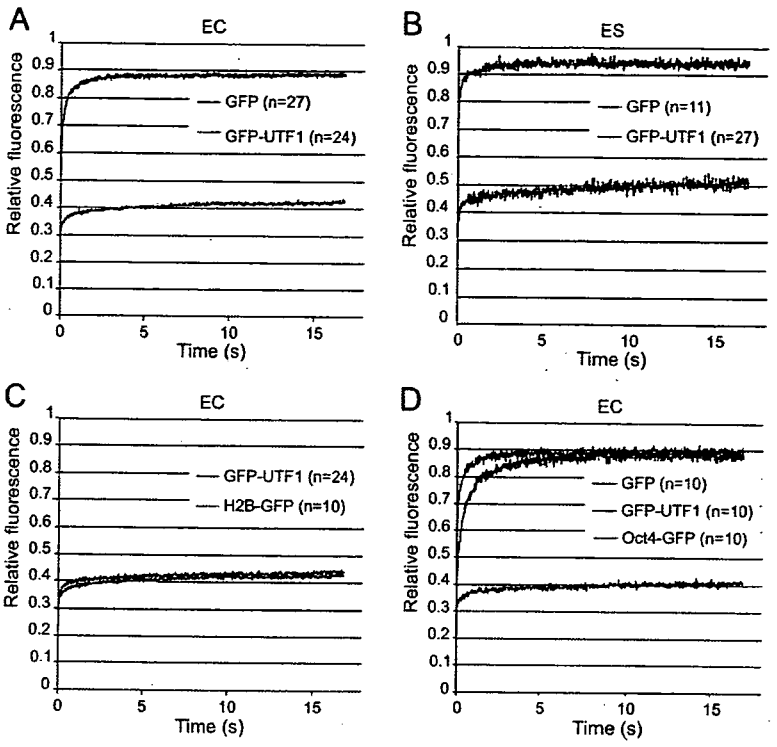

Figure 4. **Strip-FRAP analysis of GFP, GFP-UTF1, H2B-GFP, and Oct4-GFP.** (A) FRAP analysis of EC cells expressing GFP (green line) or GFP-UTF1 (blue line). The graph shows the relative fluorescent recovery directly after bleaching. The prebleach level is normalized to 1. GFP displays a quick fluorescent recovery in the bleached region, whereas GFP-UTF1 shows only little recovery directly after photobleaching. (B) FRAP analysis of ES cells expressing GFP (green line) or GFP-UTF1 (blue line). GFP shows a quick recovery after bleaching, whereas GFP-UTF1 displays only a marginal recovery. (C) FRAP experiment of EC cells expressing either GFP-UTF1 (blue line) or histone H2B-GFP (red line). GFP-UTF1 and H2B-GFP both show only a small recovery directly after photobleaching. (D) FRAP experiment of EC cells expressing GFP (green line), GFP-UTF1 (blue line), or Oct4-GFP (red line). Oct4-GFP shows a quick recovery after fluorescence, although slower than GFP.

by the cotransfection of either Smad3 and 4 (SBE) or Smad1 and 4 (BRE; Fig. 2, C and D). Cotransfection of UTF1 reduced the activity of Smad-stimulated SBE and BRE reporters by approximately twofold and fourfold, respectively. These data indicate that UTF1 is a transcriptional repressor.

Mapping of UTF1 repressor domains

UTF1 contains two conserved domains (CDs): CD1 (aa 55–124), which shares high homology with Myb/SANT DNA-binding domains, and CD2 (aa 271–334), which contains a putative leucine zipper. To identify its repressor domains, the effect of a series of GAL4-UTF1 (deletion) constructs was tested on a thymidine kinase (TK) luciferase reporter containing five copies of the GAL4 target sequence (UAS-TK-Luc; Fig. 2 E). As expected, UTF1 repressed UAS-TK-Luc reporter activity (eightfold reduction compared with GAL4). Deletion of the very C-terminal 39 aa resulted in an almost 2.8-fold reduction in repressor activity. Further C-terminal deletions only marginally affected repressor activity, but when the Myb/SANT domain (aa 55–124) was deleted, an additional drop in repressor activity compared with the 1–167 and 1–134 constructs was observed. The finding that both the C terminus and Myb/SANT domain are involved in transcriptional repression was confirmed using a series of progressive N-terminal deletions. Deletion of aa 1–65 resulted in a 3.1-fold reduction of repressor activity (compare 1–339 with 66–339), and further N-terminal deletions did not affect UTF1 repressor activity except for the deletion construct (297–339) that misses part of the CD2 domain, which completely lacked repressor activity. To address the importance of the Myb/SANT domain, we generated a mutant lacking this region, which reduced repressor activity by 1.7-fold, indicating that it is important for transcriptional repression by UTF1. In addition, the Myb/SANT domain alone (33–134) also displayed considerable repressor activity (3.9-fold repression). Collectively, these experiments indicate that both the Myb/SANT domain and the extreme C terminus of UTF1 are important for transcriptional repression by UTF1.

Live cell distribution of UTF1

To study its localization in living cells, UTF1 was fused to enhanced GFP (eGFP), creating eGFP-HA-UTF1 (hereafter GFP-UTF1), and was stably expressed in EC cells. To prevent localization artifacts, we used a clone that underexpressed GFP-UTF1 compared with the endogenous protein (Fig. 3 A). Subnuclear fractionation showed that GFP-UTF1, like endogenous UTF1, is almost exclusively found in the strongly DNA-associated fraction (Fig. 3 B). Reporter (UAS-TK-Luc) assays in HepG2 cells showed that GFP-UTF1 acted as a transcriptional repressor as well (see Fig. 5 A). These data indicate that fusing GFP to the N terminus of UTF1 does not interfere with the function of the protein.

Confocal microscopy of living cells showed that GFP-UTF1 localized to the nucleus with an inhomogeneous distribution in a similar fashion as the endogenous protein (Figs. 2 A and 3 C). GFP-UTF1 is excluded from the nucleoli (Fig. 3 C, arrows). The punctate localization is more intense around the nucleoli and in the nuclear periphery. Time-lapse imaging of a cell counterstained with Hoechst showed the chromosomal localization of GFP-UTF1 during metaphase, anaphase, and telophase (Fig. 3, D and E).

In ES cells, a similar GFP-UTF1 distribution was observed: localized to the nucleus, excluded from the nucleoli (Fig. 3 C, arrows), and chromosome associated during mitosis (Fig. 3 F, arrowhead). GFP-UTF1 ES cells were AP positive (Fig. 3 G) and expressed Oct4 (not depicted). Fractionation of GFP-UTF1 ES cells showed that both endogenous UTF1 (αmUTF1) and GFP-UTF1 (αHA) localized to the fraction containing strongly DNA-associated proteins (Fig. 3 B).

Mobility of UTF1 in living cells

To study the observation that UTF1 is a stably chromatin-associated protein in a more physiological context, we analyzed the dynamic properties of UTF1 in living cells using a FRAP protocol. In EC cells, GFP-UTF1 molecules were bleached in a small strip spanning the nucleus, and subsequent fluorescent recovery in the strip was measured at 20-ms intervals (Hoogstraten et al., 2002; van den Boom et al., 2004). The mean fluorescence intensity in the strip of several cells was plotted against time relative to the prebleach level. GFP-expressing cells showed a fast recovery of fluorescence in the strip (Fig. 4 A, green line), indicating a highly mobile protein. Fluorescence in the strip did not recover to prebleach levels as a result of the permanent bleaching of a fraction of the molecules. In contrast to GFP, GFP-UTF1 (Fig. 4 A, blue line) showed only little recovery after bleaching, indicating that the vast majority is long-term immobilized, at least for the duration of the FRAP experiments. Because mobility measurements of GFP and GFP-UTF1 in ES cells produced identical results (Fig. 4 B, green line and blue line, respectively), EC cells were used for all subsequent mobility measurements.

In terms of localization (Figs. 2 A and 3 C) and subnuclear fractionation behavior (Fig. 2 B), UTF1 greatly resembles core histones (Kanda et al., 1998). To further substantiate this observation, the mobilities of UTF1 and core histone H2B (Kimura and Cook, 2001) were compared (Fig. 4 C). FRAP curves for GFP-UTF1 (Fig. 4 C, blue line) and H2B-GFP (Fig. 4 C, red line) were virtually identical, indicating the similar molecular kinetics of these proteins. Computer simulations of the FRAP procedure were used to fit the experimental data, yielding diffusion constants, immobile fractions, and residence times of all proteins tested (Table I and Fig. S1, available at http://www.jcb.org/cgi/content/full/jcb.200702058/DC1). Both the population of GFP-UTF1 and H2B-GFP molecules displayed an immobile fraction of ~90% (Table I and Fig. S1, A and B). The duration of immobilization was much longer than the 20-s time scale of our experiments and, therefore, could only be determined with limited accuracy. For both GFP-UTF1 and H2B-GFP, a residence time in the order of minutes to hours was determined, which is in agreement with the findings of Kimura and Cook (2001).

Subsequently, we compared the dynamic behavior of GFP-UTF1 and Oct4-GFP (Fig. 4 D). In contrast to GFP-UTF1 (Fig. 4 D, blue line), Oct4-GFP (Fig. 4 D, red line) is largely mobile. Note that Oct4-GFP fluorescence recovery is much slower than that of GFP (Fig. 4 D, green line). Computer simulations indicated that 10% of the Oct4-GFP molecules are immobile with a residence time in the order of 0.1 s (Table I and Fig. S1 C). In addition, the diffusion rate of Oct4-GFP (3 $\mu m^2/s$) suggested that the protein resides in a high molecular weight complex. The highly dynamic behavior of Oct4-GFP molecules is similar to what is found for several other DNA transacting factors like the transcription/repair factor TFIIH, the homologous recombination protein Rad54, and TFIIB during interphase (McNally et al., 2000; Phair and Misteli, 2000; Chen et al., 2002; Essers et al., 2002; Hoogstraten et al., 2002; Phair et al., 2004; van den Boom et al., 2004; Houtsmuller, 2005). These data indicate that the dynamic behavior of UTF1 is similar to that of core histones but not to that of transcription factors like Oct4.

Table I. **Diffusion constants, immobile fractions, and residence times of tested constructs derived from FRAP data fitting**

Protein	Diffusion constant	Immobile fraction	Residence time
	$\mu m^2/s$	%	s
GFP	14 ± 1.8	0	0
Oct4-GFP	3 ± 1.30	10 ± 0.1	0.1 ± 0.2
H2B-GFP	1 ± 0.38	90 ± 0.01	1,024 ± 105
GFP-UTF1	0.6 ± 2.74	90 ± 0.02	512 ± 35
GFP-UTF1 W63G E67K	0.6 ± 0.5	60 ± 0.04	1,024 ± 95
GFP-UTF1 1-300	14 ± 2.74	85 ± 0.01	0.25 ± 0.04
GFP-UTF1 W63G E67K 1-300	14 ± 2.40	25 ± 0.04	0.25 ± 0.03

Localization and mobility of GFP-UTF1 mutants

Using GAL4-UTF1 fusions, we identified the putative Myb/SANT domain and the C terminus of UTF1 as repressor domains (Fig. 2 E). To investigate the requirement of these domains in UTF1 localization and mobility, a series of GFP-UTF1 mutants was generated. First, the repressor activity of wt and mutant GFP-UTF1 proteins was determined in reporter assays. Mutation of aa 63 (W→G) and 67 (E→K; GFP-UTF1 W63G E67K; Fig. 5 A), two amino acids highly conserved in Myb/SANT domains, and/or deletion of the C-terminal 39 aa (GFP-UTF1 W63G E67K 1–300; GFP-UTF1 1–300) resulted in a complete loss of UTF1 repressor activity (Fig. 5 A).

In terms of localization, GFP-UTF1 and GFP-UTF1 W63G E67K display a similar distribution. Deletion of the entire Myb/SANT domain resulted in an almost completely cytoplasmic localized fusion protein (unpublished data). GFP-UTF1 1–300 also interacted with mitotic chromosomes, whereas during interphase, the protein seemed to be more dispersed (Fig. 5 B). GFP-UTF1 W63G E67K 1–300 showed a completely homogenous nuclear distribution in combination with nucleolar exclusion. Furthermore, association with mitotic chromosomes was never observed (Fig. 5 B). These data indicate that both the Myb/SANT domain and C terminus of UTF1 are required for proper localization of the protein during interphase as well as mitosis.

To determine the role of the Myb/SANT domain and C terminus in UTF1 mobility, FRAP analyses were performed. GFP-UTF1 W63G E67K–expressing cells showed an increased recovery of fluorescence in the strip (Fig. 5 C, red line) compared